A joint special edition on

Sea Level Rise

Image credit: US National Park Service

CLIVAR *Exchanges*
No. 74 • February 2018
ISSN No: 1026-0471

US CLIVAR *Variations*
Winter 2018 • Vol. 16, No. 1
DOI: 10.5065/D6445K82

Table of Contents

US CLIVAR VARIATIONS

Editor: Kristan Uhlenbrock
US CLIVAR Project Office
Washington, DC, US
202-787-1682
www.usclivar.org

CLIVAR EXCHANGES

Editor: Jose Santos
International CLIVAR Project Office
Qingdao, China
www.clivar.org

Special thanks to Nico Caltabiano.

Sea Level Rise

Guest editor:
John Church
University of New South Wales, Australia

In June 2006, the World Climate Research Programme (WCRP) convened its first sea level workshop at the Intergovernmental Oceanographic Commission (IOC) headquarters in Paris. The workshop recognized the interdisciplinary nature of sea level change, and together with the conference statement and subsequent book, outlined progress, observational requirements, and challenges and helped stimulate further work.

Since then, there has been great progress across the full range of disciplines. This is perhaps best exemplified in closing the sea level budget over multiple timescales (requiring progress in all elements of sea level science), developing the methodology for providing regional projections (see IPCC report chapter 13), and the improved ability to simulate global and regional sea level change. Sea level change and the closely related Earth's energy budget are now recognized as central elements in understanding climate change and its impacts.

This joint publication between International and US CLIVAR begins with highlights of recent scientific progress on sea level rise research from the 2017 WCRP/IOC Sea Level Conference, and includes new estimates of historical change, evaluation of our ability to simulate it, analysis of extreme events and surface waves, and examples of the impacts.

This progress in understanding has been accompanied by a greater societal interest in sea level change as the world recognizes the vulnerability of the natural environment, increasing coastal populations, and infrastructure to rising seas.

This recognition brings new challenges. There is a need for better understanding of past and future regional change, extreme events, surface waves, and coastal impacts. Central to these issues is the long timescale of committed sea level change and how to quantify the potential for a substantially larger rise associated with the long tails of sea level (and particularly ice sheet) projections. Unfortunately, we currently have insufficient knowledge of these long tails, making probabilistic projections problematic. Attribution of sea level rise to mechanisms and the drivers of change offer the prospect of constrained projections.

Perhaps the most difficult challenge of all is engagement with the full range of stakeholders to ensure that appropriate climate change mitigation and adaptation plans are implemented in a timely fashion. This will require an informed scientific community willing to reach out well beyond their scientific disciplines.

Highlights from the WCRP/IOC Sea Level Conference July 2017, New York

Detlef Stammer[1], Robert J. Nicholls[2], and Roderik S.W. van de Wal[3]

[1]University of Hamburg, Germany
[2]University of Southampton, UK
[3]Utrecht University, The Netherlands

Anthropogenic sea level rise threatens coastal communities around the world and will continue to do so for centuries to come. To meet urgent societal needs for useful information on sea level rise, the World Climate Research Program (WCRP) has established the theme "Regional Sea Level Change and Coastal Impacts" as one of its cross-cutting "Grand Challenge" science questions. The Grand Challenge on Sea Level has developed an integrated interdisciplinary program on sea level research, reaching from the global to the regional and coastal scales, which is essential to understand impacts and adaptation needs. The program is fostering close interaction with coastal stakeholders to make sure that the results can effectively support impact and adaptation assessment efforts, as well as wider coastal zone development and management activities.

Coasts are vulnerable places due to the combination of rising sea levels and extreme events, such as storm surges and waves. Many coastal areas have dense and growing populations and economies, and host important ecosystems. Major human and economic losses have occurred in the last two decades due to storm surges: e.g., nearly 2,000 deaths and over $100 billion losses during Hurricane Katrina (US 2005) and over 100,000 deaths during Cyclone Nargis (Myanmar 2008).

Just over a decade after the first WCRP sea level conference, and three years after the 5th Assessment Report of the Intergovernmental Panel on Climate Change was published, the WCRP and the Intergovernmental Oceanographic Commission of UNESCO (IOC) organized an international conference on sea level research to address the challenges in describing and predicting regional and local sea level changes, to discuss intrinsic uncertainties, and to identify stakeholder needs for coastal planning and management.

The five-day WCRP/IOC Sea Level Conference was held at Columbia University in New York. More than 350 participants from 42 nations attended the event (Figure 1). Participant expertise was diverse, including natural scientists, social scientists, coastal engineers, managers, and planners. The conference provided a comprehensive summary of the state of climate-related, large-scale sea level research that resulted in a conference statement, which was signed by more than 350 scientists worldwide.

Conference highlights

Conference participants recognized that the present state of science provides unambiguous evidence that sea level is increasing, that sea level rise has accelerated over the past 100 years due to global warming, and that this acceleration will continue with unmitigated emission scenarios. Sea level rise represents a major challenge for coastal societies; thus, scientists must closely collaborate with the stakeholder community to further the understanding on regional mean sea level, extreme states, and future projections, develop plans for responding to change, and implement adequate adaptation measures. These collaborations are essential for assessing sea level rise impacts, as well as for enhancing climate mitigation and adaptation measures over the short-, medium- and long-term. Without urgent and significant mitigating action to combat climate change, continued greenhouse gas emissions will almost certainly commit the world to several meters of sea level rise in the next few centuries.

While global sea levels have varied by more than 100 m over geological scales, sea level has been relatively stable for the past 2,000 years. However, global sea levels started to rise around the mid 19th century and increased by about 14 to 17 cm during the 20th century. The two largest contributions to this rise have been the expansion of the ocean as it warms and the addition of mass from melting glaciers, with an increasingly larger contribution from the major ice sheets. Due to ongoing climate change, sea level rise is accelerating and currently occurs at a rate of about 30 cm per century.

If greenhouse gas emissions continue without mitigation, global sea levels could rise one meter or more throughout the 21st century, several meters by 2300, and many meters over longer timescales. With substantial and sustained reductions in greenhouse gas emissions, these changes could be greatly reduced, but even then

Figure 1. Group photo of Sea Level Conference participants taken at Columbia University.

sea level would continue to rise for many centuries. The largest uncertainty and concern in this respect is the stability of the ice sheets in Greenland and Antarctica. Substantial mass loss from these ice sheets would have significant consequences for global sea level rise and coastal communities.

The conference showcased not only the state of knowledge but also where we can direct future research.

Paleo sea level change analyses provide important data and show that (i) the paleo sea level budgets and rates need further analysis and refinement, and (ii) dynamic mantle topography is more important than previously thought over timescales of thousands of years or more, requiring additional investigation, particularly around past sea level high stands.

While the physical understanding of the ice sheets has improved, ocean–ice interactions remain poorly constrained. Scientists have a better understanding of the role of grounding lines, but questions related to buttressing and ice shelf stability remain very uncertain.

There is improved closure of the 20th century sea level budget, due to better resolution of *in situ* and satellite measurements, indicating a better understanding of its different components. Despite this progress, we still lack information on sea level change at regional scales and in coastal zones. In addition, the contributions from the deep ocean and regions covered by sea ice remain unresolved.

Our understanding of extreme sea levels is improving. Trends in extremes largely follow mean sea level changes, and elevated local sea level can often be related to climate modes (e.g., the North Atlantic Oscillation and El Niño). Pilot forecasts of monthly sea levels across the Pacific are encouraging in the prediction of extremes linked to coastal flooding. Storm surge global-scale modeling has progressed greatly, although representing the effects of tropical storms still remains challenging. Improvement in wave modeling is still limited: the first ensembles of wave projections exist, but uncertainties remain large and further development is required.

The availability of high-resolution regional sea level projections is important for science and decision-makers alike. Probabilistic descriptions of sea level rise incorporating regional details combined with information about flood recurrence frequencies are useful tools to communicate projected changes to stakeholders. Nonetheless, the future behavior of ice sheets remains an area of uncertainty, and there is considerable disagreement within the community on the shape of the tails of the sea level rise probability distribution for the second half of this century and beyond.

Impact and adaptation assessments and planning require consideration of a range of different drivers — mean changes (including uplift/subsidence), extremes, and waves. Evolving data and model systems have the potential to provide these drivers if ongoing research efforts are sustained. For example, human-induced land subsidence is a major problem in some coastal areas, especially in coastal cities located in deltas. Historic changes in subsidence have, in some local regions, greatly exceeded climatically driven mean sea level rise, and this may continue through the 21st century. These regions will require adaptation measures, many of which are defined and available. Furthermore, observations of human response to past subsidence provide a useful analogue for human response to climate-induced sea level rise, which can be exploited in the future.

Future requirements

The major and immediate climate-related impacts of sea level rise occur due to the increased likelihood of extreme sea level events, arising from the combination of high tides, storm surges, and waves on top of higher sea levels. This increased frequency of extreme sea level events and increased impact of storm surges and waves are already being observed, including routine flooding during spring tides at some locations. Hence, we think it's critical to understand the present and future occurrence

of extreme conditions in addition to mean sea level rise. Coastal impacts will not only depend on sea level rise but will also be heavily influenced by the strong socio-economic trends in coastal areas (expanding populations, urbanization, etc.), which will almost certainly continue in the coming decades. The consequences of higher sea levels will disproportionality affect the poor and vulnerable.

If the world does not respond to the challenges of sea level rise, impacts are likely to be severe. Both climate mitigation to reduce emissions and adaptation to deal with rising sea levels are needed. There are many possible adaptation measures, which, when planned appropriately, are highly effective in managing coastal risks and impacts.

To address these challenges, we recommend an internationally coordinated, new sea level change program, building on the WCRP Grand Challenge, including the provision of appropriate climate services as part of a wider sea level rise impact and adaptation effort. This program should be designed collaboratively among the global science community and user communities to serve the needs of local to national stakeholders, as they cope with present and future sea level risks.

As organizers of the conference and on behalf of the participants, we call for:

- A commitment to sustained and systematic global and regional sea level observations, including the different components (e.g., cryosphere, ocean heat content and other relevant ocean parameters, land hydrology).
- The implementation of new observations where necessary, making use of both remotely sensed and *in situ* observations. Special emphasis should be given to the monitoring of coastal regions worldwide, where a variety of climate- and non-climate-related processes interact. These observations can provide early warnings of sea level rise acceleration.
- Additional paleo data — particularly local evidence in the polar regions — in conjunction with better Earth, ice sheet, and sea level models are needed both to characterize the natural variability and non-anthropogenic contributions to ongoing sea level rise and to develop a better understanding of sea level high stands, rates of change, and ice-sheet behavior in past states of the world.
- A broad-scale assessment of uplift/subsidence, especially human-induced subsidence, to guide analysis of regional sea level change.
- The development of improved sea level forecasts and projections for planning, early warning, adaptation, and mitigation. The time frame should extend beyond 2100 to highlight the evolution of sea level, acknowledging sea level rise will not end at the end of this century.
- Improvements of our understanding of the physics of ice sheets for better projections of their contributions to future sea level change.
- An open climate model development effort — based on a range of models with advanced process parameterizations and enhanced calibration by observations — to produce improved regional and coastal sea level information, including storm surges, waves, subsidence, and land water storage at high-resolution in support of the needs of stakeholders.
- Development of a stakeholder forum that enables timely and effective exchange of vital information for mitigation of and adaptation to sea level change, including present states of and projected changes in mean and extreme sea levels, wave conditions, and potential impacts (e.g., flooding, erosion, and saltwater intrusion).
- Development of policies and regulatory frameworks for impact and adaptation assessments for all vulnerable coastal areas, such as major cities, deltas, and islands.

For more outcomes from the conference and citations for the above highlights, visit sealevel2017.org.

A reconciled estimate of 20th century global mean sea level rise

Sönke Dangendorf[1] and Marta Marcos[2,3]

[1]University of Siegen, Germany
[2]Mediterranean Institute for Advanced Studies, Spain
[3]University of the Balearic Islands, Spain

Due to its close linkage to changes in ocean heat content and melting land ice, global mean sea level (GMSL) is one of the key climate change indicators. While the modern observing system of altimetric satellites, ARGO floats (providing temperature and salinity measurements for the top 2000 m), and the Gravity Recovery and Climate Experiment (GRACE) (providing mass changes in the ocean and over the continents) provides global coverage of the spatially and temporally highly variable mean sea level (MSL) and its components, before 1992 the estimation of GMSL changes relies on a sparse set of tide gauges situated along the coast of the continental margins. Reconstructing GMSL from these tide gauges is a challenging task for a number of different reasons:

1. Tide gauges measure sea level relative to the land on which they are grounded and are, therefore, highly sensitive to the effects of vertical land motion (VLM) (Wöppelmann and Marcos 2016), which can be either induced by glacial isostatic adjustment (GIA, Peltier et al. 2004) and/or local effects such as groundwater depletion, earthquakes, etc.
2. There is no global reference system to which tide gauges measure sea level and the national datums vary widely.
3. As pointwise measurements, tide gauges track local sea levels, which reflect the geographical patterns induced by ocean dynamics and geoid changes in response to mass load redistribution (Kopp et al. 2015).

Over the past decades, many studies have been devoted to the development of different GMSL reconstruction procedures, which range from weighted averaging schemes of coastal MSL along certain coastline stretches (e.g., Jevrejeva et al. 2014) to more complex procedures where principle components of satellite altimetry are combined with tide gauges to reconstruct GMSL fields having the same spatial resolution as satellite altimetry and the same temporal coverage of tide gauges (e.g., Church and White 2011; Ray and Douglas 2011). These "classical" reconstruction procedures (which all apply GIA corrections at individual locations as the only source of VLM) generally agree on the rate of 20th century GMSL rise before 1990 with numbers between ~1.5 to 2 mm yr^{-1} and also resemble the rates inferred from satellite altimetry since 1993 within their specific uncertainties (Figure 1). Recently, Hay et al. (2015) developed a novel series of approaches based on Kalman filters and Gaussian Process Regression, which take for the first time the geographical patterns of each individual MSL

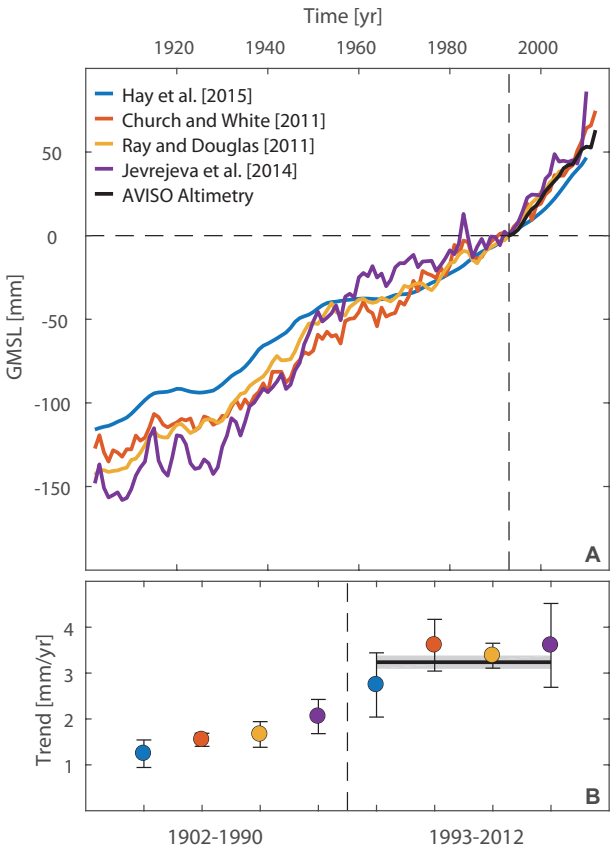

Figure 1. a) Different GMSL reconstructions over the common period from 1902 to 2012. All series have been adjusted to be zero in 1993 (dashed lines). Also shown is the GMSL as estimated from the AVISO satellite altimetry product (black line; Ablain et al. 2015). b) Linear trends of all reconstructions for two different periods (1902–1990 and 1993–2012). The black line corresponds to the linear trend of AVISO satellite altimetry during 1993-2012.

contributor into account, and came up with a significantly smaller pre-altimetric GMSL rate of 1.2 ± 0.2 mm yr^{-1} independent from the chosen tide gauge dataset (Hay et al. 2017). These lower numbers have stimulated discussions within the community (Hamlington and Thompson 2015; Thompson et al. 2016; Hay et al. 2017), but they are generally more consistent with observations and historical climate model simulations of individual contributions to the GMSL budget (Hay et al. 2015; Dangendorf et al. 2017; Slangen et al. 2017).

In this contribution, we present a novel "hybrid approach," which integrates the virtual station approach by Jevrejeva et al. (2014) with known geometries of 20th century ice melt and VLM at certain locations, two methodological adjustments for the reference frame problem and the spatial weighting of individual records. The robustness of the new "hybrid approach" is first demonstrated in realistic modeled sea level fields, where the GMSL is a priori known. Then a series of tests were conducted to explain possible reasons of differences to former assessments.

Data and approach

Our "hybrid approach" is methodologically based on the virtual station technique from Jevrejeva et al. (2006, 2014). This technique divides a sample of tide gauge records in different geographic regions. In each region, tide gauge records are aggregated into regional means by recursively combining two close sites to a new virtual station located halfway until only one virtual station, representative for the whole region, is left. The GMSL is afterwards estimated from the non-weighted average over all regions. However, as introduced above, there are at least three major challenges in such a reconstruction process.

First, tide gauges are prone to VLM. Due to the shortness and sparseness of GPS records, Jevrejeva et al. (2014) only accounted, as other earlier studies (e.g. Church and White 2011; Ray and Douglas 2011), for the modeled contribution of GIA. However, in recent years much progress has been made in directly estimating VLM at individual tide gauge locations around the world (Santamaria et al. 2017) and, consequently, nowadays a much larger set of tide gauges with robust VLM estimates has become available (Wöppelmann and Marcos 2016). In this study, we made use of these achievements and use the tide gauge subset from Wöppelmann and Marcos (2017), for which the uncertainties of VLM estimates are below 0.7 mm yr^{-1}. This resulted in a final set of 322 stations (see Dangendorf et al. 2017 for further details).

The second challenge is related to a missing common vertical reference datum for all tide gauge records around the world. Jevrejeva et al. (2006, 2014) (as many others) overcame the datum problem by reconstructing the global mean from rates and integrating the final global average back to a GMSL curve. However, Ray and Douglas (2011) discussed the concern that small errors in individual tide gauge records or the estimation of the global mean from these records may grow during the integration process and lead to drifts, especially in the earlier decades. In our sensitivity studies, we found similar signs of such drifts in our reconstructions after averaging the rates (see Dangendorf et al., 2017 for further details). Therefore, instead of averaging rates, we applied a different approach in which we first removed a common mean over at least 19 overlapping years before stacking two records into a virtual station. This avoids the integration process and the related error inflation backwards in time.

The third challenge is that, even once corrected for VLM, tide gauges track local sea level signals, which reflect the geographical patterns of ice melt fingerprints (Riva et al. 2011) and ocean dynamics, and might significantly bias the resulting regional and global averages. To minimize potential biases from the geographical patterns, each individual tide gauge record was first corrected for known geoid fingerprints from 20th century glacier melting (Marzeion et al. 2015), Greenland ice melt (Kjeldsen et al. 2016), Anarctic ice melt (Frederikse et al. 2016), groundwater depletion (Veit and Conrad 2016), and water impoundment behind dams (Fiedler and Conrad 2010) — all of which are available over the common period from 1902–2012 (see Dangendorf et al. 2017 for further details). To minimize potential regional biases stemming from ocean dynamics, we divided the ocean in six regions, which have been identified to share a common signal of decadal variability (Thompson and Merrifield 2015). This has two advantages. First, redistribution processes between these co-varying regions are averaged out. Second, the area of each region for which the virtual station is representative is now known, which was not the case in the traditional approach developed by Jevrejeva et al. (2006). Within the geographic area, a further regional weight can be applied averaging the six virtual stations to the final GMSL curve.

Results

To test the general performance of our new "hybrid approach," we conducted a series of different sensitivity experiments, which are summarized in Figure 2 and from which more detailed analyses can be found in Dangendorf et al. (2017). In the sensitivity experiments,

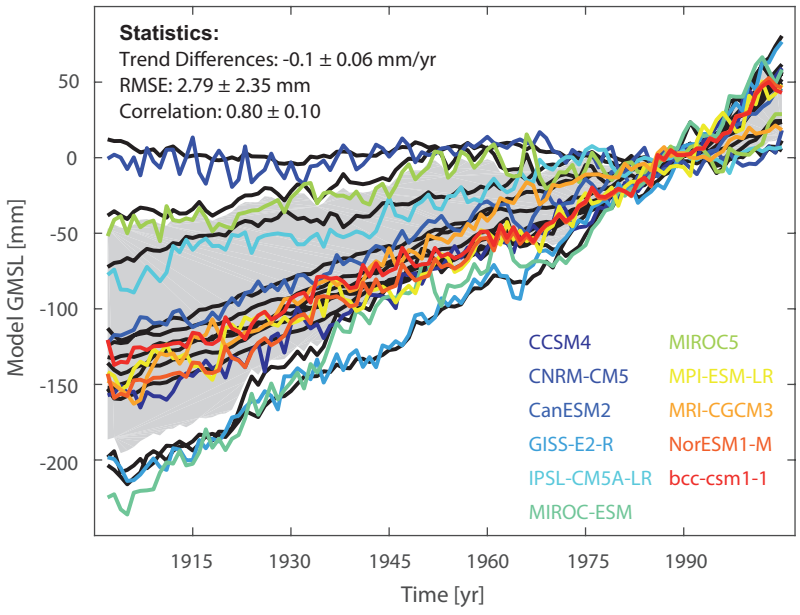

Figure 2. Results of the sensitivity experiments in CMIP5 models. Black lines represent the "true" GMSL from each model. The grey shaded area marks the 68% confidence bounds of the entire model ensemble. Reconstructions based on individual grid point time series next to the real tide gauge locations with the new hybrid approach are colored depending on the respective climate model.

we produced 11 artificial global sea level fields. These fields consist of an ocean dynamic component from historical runs of the Climate Model Intercomparison Project (CMIP5) (Marcos et al. 2017), their related glacier sea level equivalents (Marzeion et al. 2012, 2015) with geographical fingerprints, as well as the same reanalyzed 20th century geoid fingerprints from ice sheets, groundwater depletion, and water impoundment behind dams. As in these artificial sea level fields, the model specific GMSL is a priori known. Therefore, we can test the performance of our new approach by reconstructing the GMSL with only those model grid point time series in closest proximity to the real tide gauge locations. These time series are further corrected with the same data gaps as in reality.

In general, our approach shows a very good performance in reconstructing GMSL in these climate models with linear trend differences of -0.1±0.06 mm yr^{-1} over the entire period from 1902–2012 (Figure 1). Although in most of these models our approach tends to slightly overestimate the true GMSL trend over the entire century, there is no significant systematic bias. The interannual GMSL variability is also well reconstructed with model dependent correlations of 0.8±0.1 and RMSEs of 2.8±2.35 mm over the whole ensemble. However, especially in the earlier decades the variability is still significantly overestimated compared to the model truth. In those periods, the spatial sampling of tide gauges is much worse than in the most recent decades, and, consequently, the interannual variability in the GMSL reconstructions contains signals stemming from local dynamic processes such as wind forcing (Calafat and Chambers 2014; Dangendorf et al. 2014). It should further be noted that, due to the low resolution of the ocean component in CMIP5 models, coastal processes are not well represented. Consequently, performance in reconstructing true interannual GMSL variability will significantly decrease in reality. However, at lowest frequencies of several decades or more (which are the focus of this study), signals should be less affected as they are usually forced in the open ocean (Bingham and Hughes 2012), which is much better resolved in climate models.

Our resulting GMSL reconstruction with real-world tide gauge data (using the subset for which VLM uncertainty is smaller than 0.7 mm yr^{-1}) is displayed in Figure 3a, indicating a linear long-term trend of 1.3±0.2 mm yr^{-1} since 1902 (here we calculate the error considering long-term memory effects as modeled by Dangendorf et al. 2015). This value is consistent with that from Hay et al. (2015) but significantly lower than those reported in all earlier approaches considered by the Fifth Assessment Report of the Intergovernmental Panel on Climate Change (Church

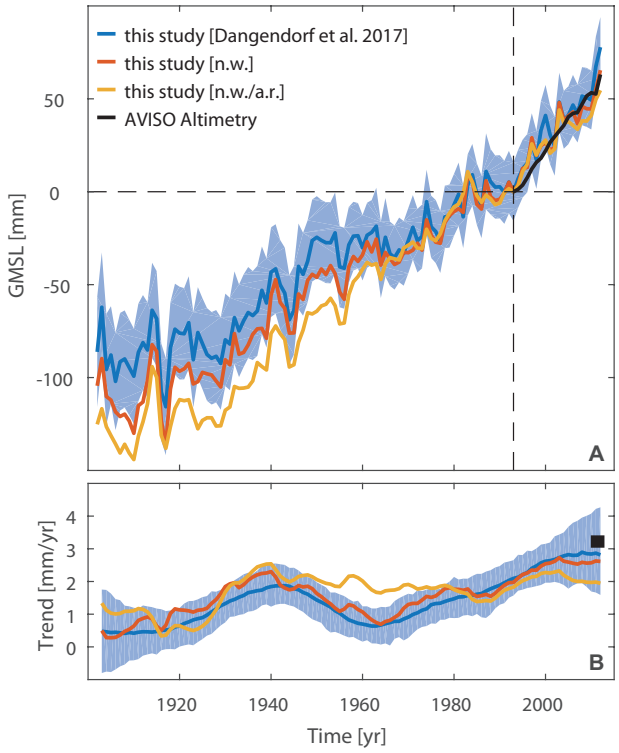

Figure 3. a) GMSL time series as reconstructed from tide gauge data (blue line). GMSL has also been reconstructed without the area weighting (n.w.; red line) as well as without the area weighting and rate averages (n.w./a.r.; yellow line). All time series have been adjusted to be zero in 1993 (dashed line). For comparison, the GMSL from AVISO altimetry is also shown (black line). The blue shading represents the 2σ uncertainties of the GMSL reconstruction. b) Nonlinear trend of time series above. The blue shading here marks the 2σ uncertainties of the rate calculation using SSA with artificial red noise. The black square corresponds to the linear trend of AVISO satellite altimetry during the period 1993–2012.

et al., 2013). The differences are particularly large before the 1970s, where the availability of tide gauge records significantly decreases in all reconstructions (Dangendorf et al. 2017; Hay et al. 2017). During the altimeter period from 1993-2012, our reconstruction yields a trend of 3.1±1.4 mm yr^{-1}, which is in close correspondence to the satellite record showing a long-term trend of 3.2±1.4 mm yr^{-1} (Figure 3b). The rates (modeled using a Singular System Analysis with an embedding dimension of 15 years (e.g., Rahmstorf et al. 2007)) of our new GMSL reconstruction show relatively constant values of ~0.5 mm yr^{-1} before the 1920s, a sharp increase to rates of ~1.8 mm yr^{-1} in the 1940s, lower rates of ~0.6 mm yr^{-1} in the 1960s, and then unprecedented high rates of ~3 mm yr^{-1} in the most recent decades (Figure 3b).

Figure 4 displays the linear trends of our new reconstruction and a selection of former assessments for the period before 1990, as this is the period where (i) largest differences between individual reconstructions emerge, and (ii) where the modeled (Gregory et al. 2012) and observed (Church et al. 2013) GMSL budget of individual contributions fell short in explaining reconstructed GMSL trends from earlier assessments. Also shown are the linear trends of the modeled CMIP5 budget as recently updated from Slangen et al. (2016). The ensemble of historical CMIP5 models shows linear trends ranging from 0.6 to 1.2 mm yr^{-1} with a median of 1 mm yr^{-1}. While Hay et al. (2015) and our new reconstruction agree with values of ~1.1-1.2 mm yr^{-1} with the upper tail of the CMIP5 trend distribution, all former assessments show significantly larger values (Figure 4).

These results raise the question of why exactly our reconstruction shows significantly smaller values than former assessments. To test for this, we performed a series of different observational sensitivity experiments. First, we subsequently tested the influence of our different methodological adjustments on pre-altimetric GMSL rates. By not accounting for the geographical area after averaging regional virtual stations into a GMSL curve, this introduces a positive drift before the 1960s (Figure 3), leading to a larger pre-altimetric GMSL trend of 1.4±0.6 mm yr^{-1} and, thus, accounting for ~0.3 mm yr^{-1} of the difference compared to former assessments (Ray and Douglas 2011; Church and White 2011; Jevrejeva et al. 2014). If we average rates instead of using a common reference datum, the resulting GMSL curve diverges even stronger from the 1970s backwards, leading to a total GMSL trend of 1.7±0.6 mm yr^{-1} before 1990, therefore explaining another ~0.3 mm yr^{-1} (Figure 3). We also tested the influence of the VLM correction instead of using GIA as in most former assessments (not shown here but visible in Figure 3b of Dangendorf et al. 2017). With the GIA correction instead of VLM, the GMSL trend again increased by ~0.3 mm yr^{-1}.

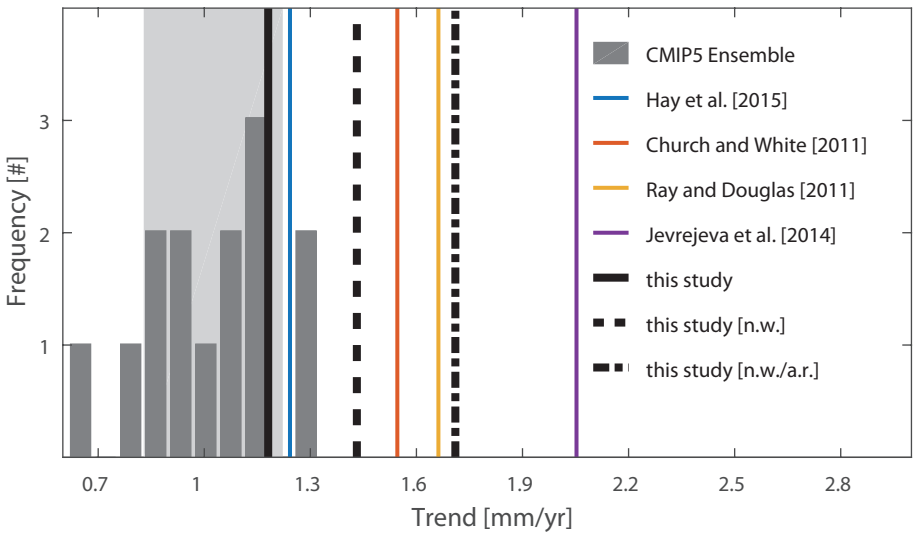

Figure 4. Linear trend frequency of different reconstructions and climate models over the period 1902–1990. The grey shading marks the 68% confidence bounds of the CMIP5 derived linear trend ensemble.

Discussion and outlook

In our contribution, we have reassessed 20th century GMSL with a novel "hybrid approach," which combines the virtual station technique from Jevrejeva et al. (2006, 2014) with known geometries of individual sea level contributors, as well as newly available VLM estimates (Wöppelmann and Marcos 2016). This minimizes the regional variability at each location, ultimately leading to an improved GMSL estimate especially in the earlier and data sparse periods. We also adjusted the technique with a different approach for overcoming the reference datum problem of tide gauge records and a new area-weighting algorithm in which the ocean is divided in six ocean basins of homogeneous decadal sea level variability (Thompson and Merrifield 2014). Altogether, these adjustments lead to a significantly smaller GMSL trend before 1990 compared to former assessments (Church et al. 2013) but are in good agreement to the most recent study of Hay et al. (2015), as well as the sum of individual contributors modeled with CMIP5 climate model outputs (Slangen et al. 2016). In a recent study, Frederikse et al. (2017) further showed that the "hybrid approach" is also able to close the observational basin-scale and global sea level budget of individual contributions since 1958 (note that there are some further adjustments in the individual tide gauge corrections compared to this assessment).

Our study sheds light on an important enigma regarding the pre-altimetric GMSL rates. Although we have demonstrated the significant influence of some widely used methodological adjustments, further assessments are required using exactly the approaches as in the different former studies (e.g., with the widely used EOF approaches, etc.). A first step in this direction has been done and an international team of experts has been formed for a large GMSL intercomparison project at the International Space Science Institute (ISSI) in Bern, Switzerland.

Acknowledgements

The authors thank the International Space Science Institute (ISSI; Bern, Switzerland) for support of the International Team "Towards a unified Sea Level Record". Dangendorf further acknowledges a visiting scientist fellowship of the University of the Balearic Islands.

References

Ablain, M. and Coauthors, 2015: Improved sea level record over the satellite altimetry era (1993-2010) from the Climate Change Initiative project. *Ocean Sci.* **11,** 67-82, doi:10.5194/os-11-67-2015.

Bingham R. J., and C. W. Hughes, 2012: Local diagnostics to estimate density-induced sea level variations over topography and along coastlines. *J. Geophys. Res.-Oceans*, **117**, doi:10.1029/2011JC007276.

Church, J. A, and N. J. White, 2011: Sea-level rise from the late 19th to the early 21st Century. *Surv. Geophys.*, **32**, 585-602, doi:10.1007/s10712-011-9119-1.

Church, J. A., and Coauthors, 2013: Sea Level Change. *Climate Change 2013: The Physical Science Basis. Contribution of Working Group I to the Fifth Assessment Report of the Intergovernmental Panel on Climate Change*. Stocker, T. F., D. Qin, G.-K. Plattner, M. Tignor, S. K. Allen, J. Boschung, A. Nauels, Y. Xia, V. Bex and P. M. Midgley, Eds., Cambridge University Press, Cambridge, UK and New York, NY, USA, doi:10.1017/CBO9781107415324.026.

Calafat, F. M., and D. P. Chambers, 2014: Quantifying recent acceleration in sea level unrelated to internal climate variability. *Geophys. Res. Lett.*, **40**, 3661-3666, doi:10.1002/grl.50731.

Dangendorf, S,. and Coauthors, 2014: Mean sea level variability in the North Sea: Processes and implications. *J. Geophys. Res. Oceans,* **119**, 6820-6841, doi:10.1002/2014JC009901.

Dangendorf S, M. Marcos, A. Muller, E. Zorita, R. Riva, K. Berk, and J. Jenson, 2015: Detecting anthropogenic footprints in sea level rise. *Nature Comm.*, **6,** doi:10.1038/ncomms8849.

Dangendorf S., M. Marcos, G. Woppelmann, Cl. P. Conrad, T. Frederikse, and R. Riva, 2017: Reassessment of 20th century global mean sea level rise. *Proc. Nat. Acad. Sci.*, **114**, 5946-5951, doi:10.1073/pnas.1616007114.

Fiedler, J. W., and C. P. Conrad, 2010: Spatial variability of sea level rise due to water impoundment behind dams. *Geophys. Res. Lett.*, **37**, doi:10.1029/2010GL043462.

Frederikse T., R. Riva, M. Kleinherenbrink. Y. Wada, M. van den Broeke, and B. Marzeion, 2016: Closing the sea level budget on a regional scale: Trends and variability on the Northwestern European continental shelf. *Geophys. Res. Lett.*, **43,** 864-872, doi:10.1002/2016GL070750.

Frederikse T, S. Jevrejeva, R. Riva, and S. Dangendorf, 2017: A consistent sea-level reconstruction and its budget on basin and global scales over 1958-2014. *J. Climate*, doi:10.1175/JCLI-D-17-0502.1.

Gregory J., and Coauthors, 2013: Global mean-sea level rise: is the whole greater than the sum of all prats? *J. Climate*, **26**, 4476-4499, doi:10.1175/JCLI-D-12-00319.1.

Hamlington, B.D, and P. R. Thompson, 2015: Considerations for estimating the 20th century trend in global mean sea level. *Geophys. Res. Lett*., **42**, 4102-4109, doi: 10.1002/2015GL064177.
Hay C. H., E. Morrow, R. E. Kopp, and J. X. Mitrovica, 2015: Probabilistic reanalysis of twentieth-century sea level rise. *Nature*, **517**, 481–484, doi:10.1038/nature14093.
Hay C. H., E. Morrow, R. E. Kopp, and J. X. Mitrovica, 2017: On the robustness of Bayesian fingerprinting estimates of global sea-level change. *J. Climate*, **30**, 3025–3038, doi:10.1175/JCLI-D-16-0271.1.
Jevrejeva S., A. Grinsted, J. C. Moore, and S. Holgate, 2006: Nonlinear trends and multiyear cycles in sea level records. *J. Geophys. Res*., **111**, doi:10.1029/2005JC003229.
Jevrejeva S, J. C. Moore, A. Grinsted, A. P. Matthews, and G. Spada, 2014: Trends and acceleration in global and regional sea levels since 1807. *Glob. Planet. Change*, **113**, 11-22, doi:10.1016/j.gloplacha.2013.12.004.
Kopp R. E., C. C. Hay, C. M. Little, and J. X. Mitrovica, 2015: Geographic variability of sea-level change. *Curr. Climate Change Rep.*, **1,** 192-204, doi:10.1007/s40641-015-0015-5.
Kjeldsen K. K., and Coauthors, 2015: Spatial and temporal distribution of mass loss from the Greenland ice sheet since AD 1900. *Nature*, **528**, 396-400, doi:10.1038/nature16183.
Peltier W. R., 2004: Global glacial isostacy and the surface of the Ice-Age Earth: The ICE5G(VM2) model and GRACE. *Ann. Rev. Earth. Planet. Sci*., **32**, 111-149, doi:10.1146/annurev.earth.32.082503.144359.
Marcos M., B. Marzeion, S. Dangendorf, A. B. Slanger, H. Palanisamy. And L. Fenoglio-Marc, 2016: Internal variability versus anthropogenic forcing on sea level and its components. *Surv. Geophys.*, **38,** 329-348, doi:10.1007/s10712-016-9373-3.
Marzeion B., A. H. Jarosch, and M. Hofer, 2012: Past and future sea-level change from the surface mass balance of glaciers. *The Cryosph.*, **6**, 1295-1322, doi:10.5194/tc-6-1295-2012.
Ray R. D., and B. C. Douglas, 2011: Experiments in reconstructing twentieth-century sea levels. *Prog. Oceanogr*., **91**, 496–515, doi:10.1016/j.pocean.2011.07.021.
Rahmstorf S., 2007: A semi-empirical approach to projecting future sea-level rise. *Science*, **315**, 368-370, doi:10.1126/science.1135456.
Slangen A. B. A., J. A. Church, C. Agosta, X. Fettweis, B. Marzeion, and K. Richter, 2016: Anthropogenic forcing dominates global mean sea-level rise since 1970. *Nature Climate Change*, **6,** 701-705, doi:10.1038/nclimate2991.
Slangen A. B. A., and Coauthors, 2017: Evaluating model simulations of twentieth-century sea level rise. Part 1: global mean sea level change. *J. Climate*, **30**, 8539-8563, doi:10.1175/JCLI-D-17-0110.1.
Thompson P. R., and M. A. Merrifield, 2014: A unique asymmetry in the pattern of recent sea level change. *Geophys. Res. Lett*., **41**, 7675–7683, doi:10.1002/2014GL061263.
Thompson P. R., B. D. Hamlington, F. W. Landerer, and S. Adhikari, 2016: Are long tide gauge records in the wrong place to measure global mean sea level rise? *Geophys. Res. Lett.*, **43**, 403-410, doi:10.1002/2016GL070552.
Veit E, and C. P. Conrad, 2016: The impact of groundwater depletion on spatial variations in sea level change during the past century, *Geophys. Res. Lett*., **43**, 3351-3359, doi:10.1002/2016GL068118.
Wöppelmann G., and M. Marcos, 2016: Vertical land motion as a key to understanding sea level change and variability. *Rev. Geophys*., **54**, 64-92, doi:10.1002/2015RG000502.

Second International Conference on Subseasonal to Seasonal Prediction (S2S) *and*
Second International Conference on Seasonal to Decadal Prediction (S2D)

Abstracts Due March 16

Evaluating climate model simulations of 20th century sea level rise

Benoit Meyssignac[1], Aimée Slangen[2,3], Angélique Melet[4], John A. Church[5], Xavier Fettweis[6], Ben Marzeion[7], Cécile Agosta[6], Stefan R.M. Ligtenberg[3], Giorgio Spada[8], Kristin Richter[9], Matt D. Palmer[10], Chris D. Roberts[10,11], Nicolas Champollion[12]

[1]LEGOS, University of Toulouse, CNES, CNRS, IRD, UPS, France
[2]Royal Netherlands Institute for Sea Research, The Netherlands
[3]Utrecht University, The Netherlands
[4]Mercator Ocean, France
[5]University of New South Wales, Australia
[6]University of Liège, Belgium
[7]University of Bremen, Germany
[8]University of Urbino, Italy
[9]University of Innsbruck, Austria
[10]Met Office Hadley Centre, UK
[11]European Centre for Medium Range Weather Forecasts, UK
[12]International Space Science Institute, Switzerland

Tide gauge records and satellite observations show that sea level has risen during the 20th century and that this rise has not been spatially uniform (Church and White 2011; Hay et al. 2015; Meyssignac and Cazenave 2012; Slangen et al. 2014b; Wöppelmann et al. 2009). Process-based projections indicate that global mean sea level rise will almost certainly accelerate through the 21st century in response to greenhouse gas (GHG) emissions and associated global warming (Church et al. 2013). However, the magnitude of this rise and its spatial variations remain uncertain because of uncertainties in the underlying physical processes, in GHG emissions, and because of inherent uncertainty associated to the chaotic nature of the climate variability.

Projections of future sea level are based on the Climate Model Intercomparison Project Phase 5 (CMIP5) simulations of the 21st century climate (Taylor et al. 2012), and their reliability and uncertainty depend on the quality of the climate models used. In two recent articles (Meyssignac et al. 2017; Slangen et al. 2017), we evaluated the ability of CMIP5 climate models to reproduce observed sea level rise over the 20th century. The objectives were i) to evaluate the climate models' ability to simulate global and regional sea level changes and to identify and understand potential limitations of these models, and ii) to determine the causes of the temporal and regional variations in the 20th century sea level rise. Here, we summarize the main findings of these two articles.

Our approach consists of estimating contributions to 20th century sea level changes, primarily using the output of the CMIP5 climate model simulations (from 12 different climate models in total). Then we add these contributions together and compare the sum with observations of sea

level changes from tide gauge records. This approach builds upon recent progress in projecting the contributions to sea level changes at regional scale from climate models (Cannaby et al 2016; Kopp et al. 2014; Perrette et al. 2013; Slangen et al. 2014a,b; Spada et al. 2013), but in this article we focus on the historical changes. We use CMIP5 climate models to directly estimate the global and regional sea level changes associated with ocean density and circulation changes ("dynamic sea level" hereafter; Lowe and Gregory 2006) and the contribution from changes in atmospheric loading (Wunsch and Stammer 1997). Glacier mass changes are estimated by driving the global glacier evolution model of Marzeion et al. (2012) with temperature and precipitation from the CMIP5 climate model simulations. Greenland ice sheet surface mass balance is estimated with a downscaling technique based on simulations of the regional climate model MAR (Modèle Atmosphérique Régional; Fettweis et al. 2017) forced with temperature and precipitation over the Greenland ice sheet from the CMIP5 simulations (Meyssignac et al. 2016). The Antarctic ice sheet surface mass balance is also estimated from CMIP5 outputs using precipitation minus evaporation over the ice sheet and neglecting the runoff of surface melt water, as it is very small under the 20th century climate (Lenaerts et al. 2012). The contribution from groundwater depletion, reservoir storage, and dynamic ice sheet mass changes are estimated from hydrological models and observations (Döll et al. 2014; Shepherd et al. 2012; Wada et al. 2016), because these processes are not included in the climate model simulations. The sea level patterns associated with changes in the mass of land-based ice and water are computed with two different sea level equation solvers (Schotman, 2008; Spada and Stocchi 2007). We also consider the contribution associated with glacial isostatic adjustment (GIA), which is the ongoing solid Earth response to the melt of the former ice sheets during the last deglaciation, using GIA-model estimates from Peltier (2004) and A et al., (2013). All contributions are then summed to provide an estimate of the global and regional sea level changes from climate models between 1900 and 2015.

To cover the period 1900–2015, the CMIP5 historical simulations (1850-2005) were extended using the Representative Concentration Pathway 8.5 scenario (RCP8.5; Moss et al. 2010). This RCP projects a nominal radiative forcing increase of ~8.5 Wm^{-2} in 2100 relative to pre-industrial conditions. The choice for the RCP8.5 scenario was based on data availability and is not critical to our results, as projections of sea level change are largely scenario independent before 2030 or so (Church et al. 2013).

We selected 27 long tide gauge records from the Permanent Service for Mean Sea Level (PSMSL 2016; Holgate et al. 2012), with the objective to get the longest high-quality tide gauge dataset covering as many regions of the world as possible. Most of the selected tide gauge records cover a period longer than 70 years. In regions where such long records could not be found, the longest record available was chosen. Tide gauges need to be corrected for vertical land movement processes, other than GIA (which is included as an offline calculation in the CMIP5 model-based sea level times series). These processes can include plate tectonics, sediment compaction, or subsidence caused by anthropogenic extraction of underground fluids. We used estimates of the vertical land movements based on GPS measurements from Wöppelmann et al. (2009) to correct the tide gauge records.

For the estimation of the observed global mean sea level change (GMSL), it is not ideal to directly use the tide gauge records because they are distributed unevenly around the world (particularly those with the longest records) and are confined to coastal locations. A simple average of the tide gauge records would result in a biased GMSL record (Thompson et al. 2016). Instead we use the GMSL reconstructions of Church and White (2011), Hay et al. (2015), Jevrejeva et al. (2014), and Ray and Douglas (2011; Figure 1). Each reconstruction uses a different method to limit biases when combining the sparse unevenly distributed tide gauge records into a global mean (see Slangen et al. 2017 for more details).

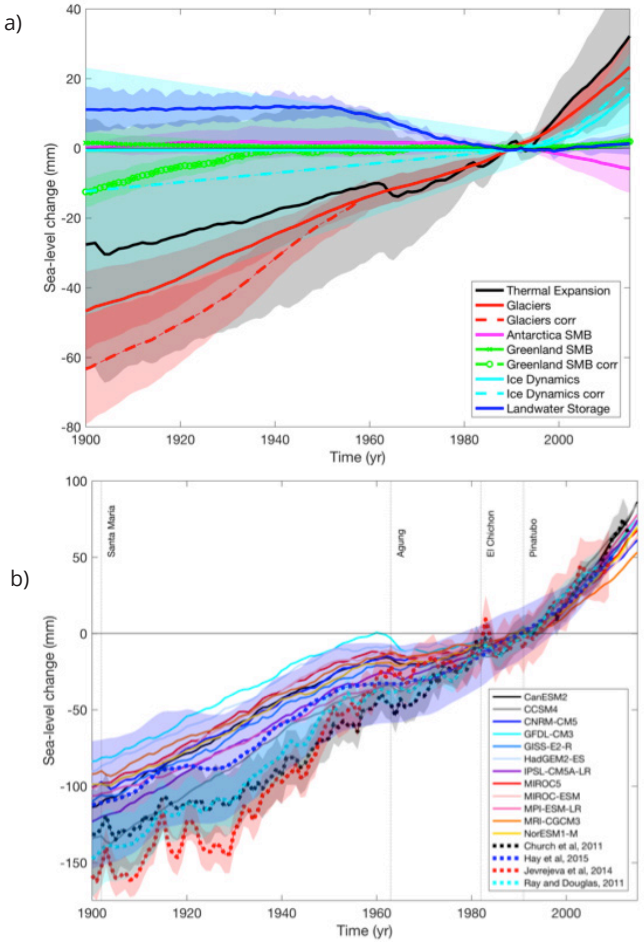

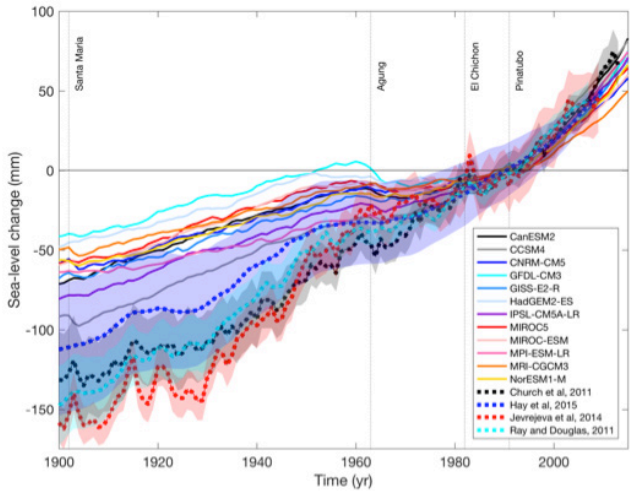

Figure 1. a) Ensemble mean of the modeled sea level contributions (1900–2015, mm), ± 1.65σ for each contribution, relative to a baseline period of 1980–2000, excluding (solid) and including (dashed) proposed corrections. b,c) Modeled total sea level change (1900–2015, mm) for 12 CMIP5 models compared to observational reconstructions, relative to a baseline period of 1980-2000, models in b) exclude and in c) include proposed corrections for glaciers and ice sheets. Observational reconstructions (dashed lines): Church and White (2011) in grey, Hay et al. (2015) in blue, Jevrejeva et al. (2014) in red, Ray and Douglas (2011) in cyan, shading indicates 1.65σ. Major volcanic eruptions indicated with dashed vertical lines.

At a global scale, when all the simulated contributions to sea level are combined together, we find a substantial gap between the observations and the models: only 50 ± 30% of the observed GMSL change (mean of four tide gauge reconstructions) can be explained by the models for the period 1901–1920 to 1988–2007 (Figure 1b). This gap comes primarily from models underestimating the contributions from glaciers and Greenland surface mass balance to GMSL changes in the first part of the 20th century. Indeed, the glacier contribution and the Greenland surface mass balance contribution are much larger in the early 20th century (1900-1940) when they are computed using temperature and precipitation fields from an atmospheric reanalysis rather than CMIP5 model estimates. This finding aligns with recent observational evidence, which points to a much larger (surface mass balance + ice dynamical) contribution from the Greenland ice sheet than previously thought (Kjeldsen et al. 2015). To correct for this bias, we propose a correction for the glacier and the Greenland surface mass balance contributions based on the differences between CMIP5 and atmospheric reanalyses (ERA-20C from Poli et al., 2016, 20CRv2 and 20CRv2c from Compo et al. 2011) driven estimates (see Figure 1a). Following Slangen et al. (2016), we also explore the possibility that ice sheets and the deep ocean are not in equilibrium with 20th century climate, as their response time is likely to be on a century-to-millennia timescale. We use a constant of 0.13 ± 0.35 mm yr^{-1} as derived in Slangen et al. (2016). The suggested bias corrections for Greenland surface mass balance, glaciers, and deep ocean/ice sheet contributions reduce the model-observation gap — as they are based on

model-observation differences — bringing the explained percentage to 75 ± 38% for the mean of the four reconstructions (Figure 1c). Compared to the individual reconstructions, the bias-corrected simulations agree best with the Hay et al. (2015) reconstruction, explaining 92% of the observed change (Figure 1c). Over the satellite altimetry period (1993–2015), the percentage change explained by the simulations is 102 ± 33% (105 ± 35% when bias corrections are included), effectively closing the sea level budget for this period.

The simulated GMSL time series show increasing decadal trends over the 20th century, due to both increasing contributions from thermal expansion and the mass components. Thermal expansion starts to contribute to GMSL from 1910 onwards, and by 2015 accounts for 46% of the total simulated sea level rise. The mass contribution, which accounts for the remaining 54% in 2015, is dominated by the glacier contribution until the ice sheet dynamics start to play a role at the end of the 20th century, accounting for 12% of total simulated GMSL in 2015. The land water contribution causes a decrease in sea level before the 1950s, due to the increasing reservoir storage, while closer to the present day the groundwater extraction increases, leading to a small and increasing positive contribution to GMSL from land water storage changes.

The ice sheet surface mass balance contributions are relatively small compared to all the other contributions, apart from the proposed bias correction to the Greenland surface mass balance component, which is of similar magnitude (but opposite sign) to the land water storage change. Finally, the ice sheet dynamical component is initially dominated by the proposed non-equilibrium term, but by the end of the 20th century the ice sheets start to show an increasing contribution from ice sheet dynamical discharge.

At a regional scale, the simulated 20th century sea level change shows substantial regional departures around the GMSL that are within ±100% of the global signal for more than 90% of the ocean (Figure 2). The largest departures from GMSL are around the former and present ice sheets (Laurentide, Fenoscandia, Greenland, and Antarctic),

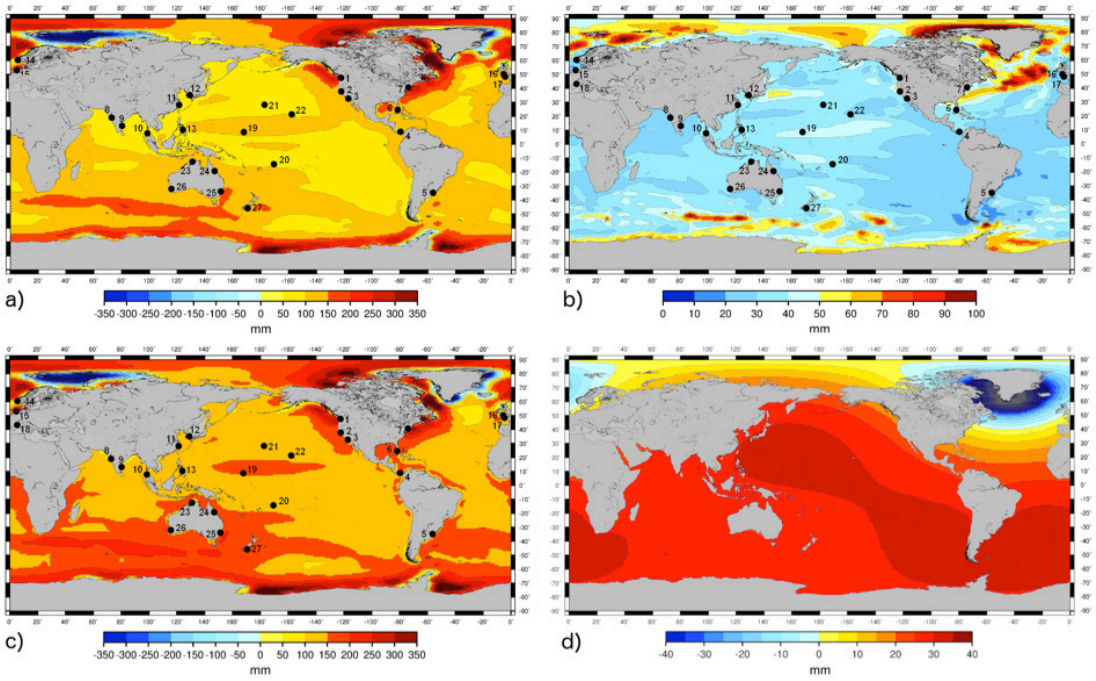

Figure 2. Simulated 20th century sea level change. a) Ensemble mean of the time-averaged total relative sea level change (mm) for 1996–2015 relative to the reference period 1901–1920. b) Root mean square spread of the individual model results around the ensemble mean (mm). c) Same as a) but includes the bias correction presented in d). d) Sea level change for the period 1996–2015 relative to the reference period 1901–1920 induced by the ice sheets/deep ocean correction plus glaciers and Greenland surface mass balance correction. The black dots on panel a) and c) indicate the position of the tide gauge records used to assess the simulated sea level from climate models. Red indicates sea level rise and blue indicates sea level fall. The hatched areas indicate regions where the ensemble mean signal is smaller than 1.65 standard deviations of the ensemble spread (i.e., the 90% CL).

and mostly explained by local vertical land movement associated with GIA. In the rest of the ocean, the spatial variations in sea level are dominated by the spatial variations in dynamic sea level. Locally around India and western United States, sea level rise has been lower than the global mean because of groundwater depletion (Figure 2).

The comparison of the simulated 20th century regional sea level changes with the selected 27 tide gauge records shows that, in general, the amplitude in the observed multi-decadal variability in sea level is well captured by the climate model ensemble (not shown here; see Meyssignac et al. 2017). This multi-decadal variability essentially comes from the dynamic sea level contribution. Its amplitude is fairly well-reproduced here because climate models have been shown to simulate the main features of the principal climate modes of variability, such as the Interdecadal Pacific Oscillation (except in the northwestern tropical Pacific; Lyu et al. 2016; Meehl et al. 2009; Power et al. 2006), the Atlantic multidecadal variability (AMV, e.g., Menary et al. 2012), or the Atlantic meridional overturning circulation (AMOC; e.g., Msadek et al. 2013). The interannual variability observed by tide gauges is only partially captured by climate models. Indeed, climate models show local deficiencies in simulating sea level changes (e.g., in the Andaman Sea). Tide gauge records also indicate that climate models tend to underestimate the sea level changes associated with extreme ENSO events on the western coast of the United States and in the Pacific islands.

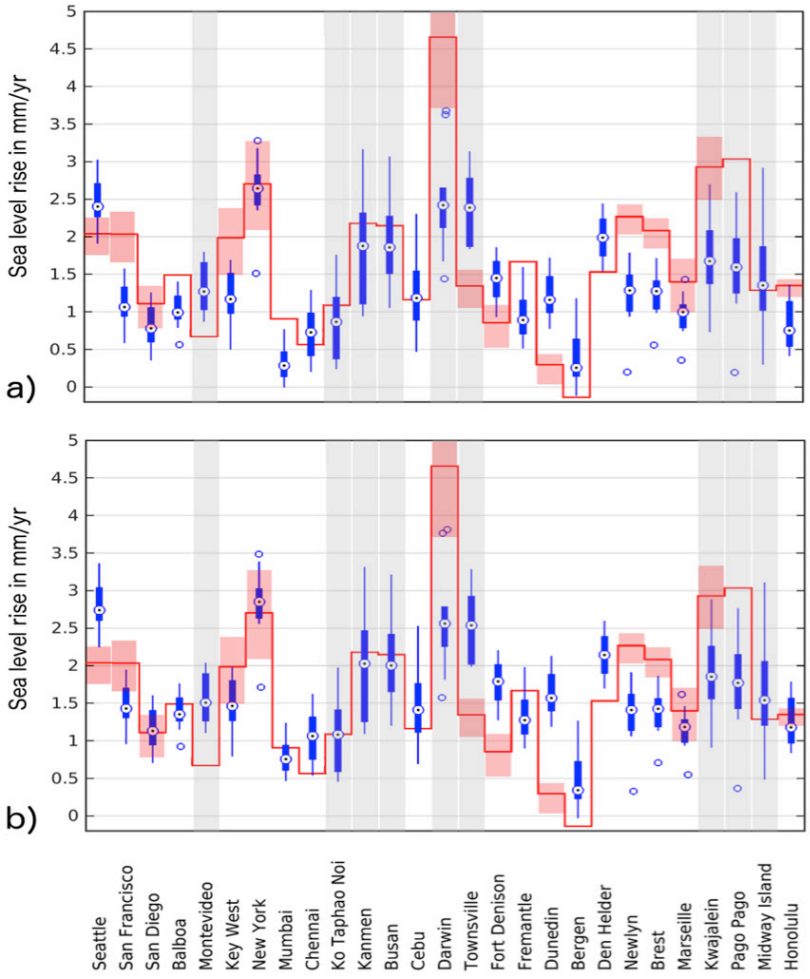

Figure 3. a) Box plot of the observed (red) and modeled (blue) sea level trends at each tide gauge station (over the tide gauge record period) in mm yr^{-1}. On each box, the blue dot inside a white circle indicates the median of the ensemble of modeled sea level trend, and the bottom and top edges of the box indicate the 75% confidence level. The whiskers extend to cover the 90% confidence level of the ensemble data (computed as the 1.65 σ assuming a normal distribution). The outliers are plotted individually using a circle. The red line indicates the observed sea level trend by the tide gauge records. The red shaded areas indicate the uncertainty in the observed tide gauge trends deduced from the formal error of the trend calculation and the formal error of the vertical land motion estimate when available. The uncertainty is sizeable only for tide gauge records with vertical land motion estimates. The grey shaded areas indicate the tide gauge records with less than 70 years. The trends of these tide gauge records are potentially dominated by decadal-to-multidecadal internal variability. b) Same as a) but after applying the correction (see text) to the ensemble of modeled sea level trends.

At the 27 tide gauge locations, climate model simulations tend to underestimate the observed 20th century long-term trends (Figure 3a). The average difference between observed and simulated sea level trends over the range of tide gauges is 0.27 ± 0.77 mm yr^{-1} (90% CL). For the records that span less than 70 years, the multi-decadal variability in the observed records potentially masks the

long-term trend, making it difficult to assess the modeled sea level. However, the long tide gauge records point to a systematic underestimation of observed sea level trends in CMIP5 simulations in the early part of the 20th century, supporting the results for GMSL. The proposed bias corrections for Greenland surface mass balance, glaciers, and deep ocean/long-term ice sheet contributions reduce the gap between models and observations of sea level (Figure 3b) and result in an average difference between observed and modeled sea level trends of 0.02 ± 0.74 mm yr^{-1} (90% CL). The bias correction also improves the spatial variability in modeled sea level trends, bringing the standard deviation of the differences between the model and individual tide gauge records from 0.77 mm yr^{-1} to 0.73 mm yr^{-1} (Figure 3b). While at low- and mid-latitudes, all tide gauge trends are better estimated when the correction is applied. At high-latitudes (e.g., Seattle, New York, or Fort Denison), the comparison between observed and simulated sea level is worse with the bias correction (Figure 3b). This indicates that while the amplitude of the proposed bias correction seems right its regional pattern needs to be improved. The discrepancy at high-latitudes suggests that the ice sheet contribution might be underestimated in the bias correction or that there is some significant error in the GIA correction. Better understanding of the GIA estimates with improved models may help in both refining the bias correction and reducing the discrepancies at high-latitudes between simulated and observed sea level. At low-latitudes, even the smaller contributions to sea level changes need to be carefully taken into account if we want to explain local deviations of the sea level trends. This is, for instance, illustrated with the groundwater depletion contribution to explain the low sea level rise observed around India.

The general fairly good agreement between regional tide gauge observations and simulations of regional sea level provides confidence in the ability of climate models to project future sea level changes, except for the contributions from ice sheet dynamics and groundwater storage (which were not simulated here). The next step is to work towards regional attribution of sea level changes.

Acknowledgements

The authors acknowledge the World Climate Research Programme's Working Group on Coupled Modelling, which is responsible for CMIP, and thank the climate modeling groups for producing and making available their model output. For CMIP, the U.S. Department of Energy's Program for Climate Model Diagnosis and Intercomparison provides coordinating support and led development of software infrastructure in partnership with the Global Organization for Earth System Science Portals. The authors thank the International Space Science Institute (ISSI; Bern, Switzerland) for support of the International Team on contemporary regional and global sea level rise. GS is funded by a DiSPeA grant of the Urbino University (CUP H32I160000000005). This work has been supported by CNES.

References

A G., J. Wahr and S. Zhong, 2013: Computations of the viscoelastic response of a 3-D compressible Earth to surface loading: an application to Glacial Isostatic Adjustment in Antarctica and Canada. *Geophys. J. Int.*, **192**, 557–572, doi:10.1093/gji/ggs030.

Cannaby, H., et al and Coauthors, 2016: Sea level rise and changes in extreme storm surge and wave events during the 21st century in the region of Singapore. *Ocean Sci.,* **12,** doi:10.5194/os-12-613-2016.

Church, J. A., and N. J. White, 2011: Sea level rise from the late 19th to the early 21st century. *Surv. Geophys.*, **32**, 585–602, doi:10.1007/s10712-011-9119-1.

Church, J. A., and N. J. White, 2011b: Sea level rise from the late 19th to the early 21st century. *Surv Geophys*, doi:10.1007/s10712-011-9119-1.

Church, J. A., and Coauthors, 2013: Sea Level Change. *Climate Change 2013: The Physical Science Basis. Contribution of Working Group I to the Fifth Assessment Report of the Intergovernmental Panel on Climate Change*. Stocker, T. F., D. Qin, G.-K. Plattner, M. Tignor, S. K. Allen, J. Boschung, A. Nauels, Y. Xia, V. Bex and P. M. Midgley, Eds., Cambridge University Press, Cambridge, UK and New York, NY, USA, doi:10.1017/CBO9781107415324.026.

Compo, G. P., and Coauthors, 2011: The Twentieth Century Reanalysis Project. *Q. J. R. Meteorol. Soc.*, **137**, 1–28, doi:10.1002/qj.776.

Döll, P., H. Müller Schmied, C. Schuh, F. T. Portmann, and A. Eicker, 2014: Global-scale assessment of groundwater depletion and related groundwater abstractions: Combining hydrological modeling with information from well observations

and GRACE satellites. *Water Resour. Res.*, **50**, 5698–5720, doi:10.1002/2014WR015595.
Fettweis X., J. E. Box, C. Agosta, C. Amory, C. Kittel, C. Lang, D. van As, H. Machguth, and H. Gallée, 2017: Reconstructions of the 1900–2015 Greenland ice sheet surface mass balance using the regional climate MAR model. *The Cryo*., **11**, 1015-1033, doi:10.5194/tc-11-1015-2017.
Griffies, S. M., and R. J. Greatbatch, 2012: Physical processes that impact the evolution of global mean sea level in ocean climate models. *Ocean Model.*, **51**, 37–72, doi:10.1016/j.ocemod.2012.04.003.
Hay, C. C., E. Morrow, R. E. Kopp, and J. X. Mitrovica, 2015a: Probabilistic reanalysis of twentieth-century sea-level rise. *Nature*, **517**, 481–484, doi:10.1038/nature14093.
Holgate, S. J., and Coauthors, 2012: New data systems and products at the Permanent Service for Mean Sea Level. *J. Coast. Res.*, 493–504, doi:10.2112/JCOASTRES-D-12-00175.1.
Jevrejeva, S., J. C. Moore, A. Grinsted, A. P. Matthews, and G. Spada, 2014: Trends and acceleration in global and regional sea levels since 1807. *Glob. Planet. Change*, **113**, 11–22, doi:10.1016/j.gloplacha.2013.12.004.
Kjeldsen, K. K., and Coauthors, 2015: Spatial and temporal distribution of mass loss from the Greenland Ice Sheet since AD 1900. *Nature*, **528**, 396–400, doi:10.1038/nature16183.
Kopp, R. E., R. M. Horton, C. M. Little, J. X. Mitrovica, M. Oppenheimer, D. J. Rasmussen, B. H. Strauss, and C. Tebaldi, 2014: Probabilistic 21st and 22nd century sea-level projections at a global network of tide-gauge sites. *Earths Future*, **2**, doi:10.1002/2014EF000239.
Lenaerts, J. T. M., M. R. van den Broeke, W. J. van de Berg, E. van Meijgaard, and P. Kuipers Munneke, 2012: A new, high-resolution surface mass balance map of Antarctica (1979–2010) based on regional atmospheric climate modeling. *Geophys. Res. Lett.*, **39**, doi:10.1029/2011GL050713.
Lowe, J. A., and J. M. Gregory, 2006: Understanding projections of sea level rise in a Hadley Centre coupled climate model. *J. Geophys. Res.*, **111**, doi:10.1029/2005JC003421.
Lyu, K., X. Zhang, J. A. Church, A. B. A. Slangen, and J. Hu, 2014: Time of emergence for regional sea-level change. *Nat. Clim. Change*, **4**, 1006–1010, doi:10.1038/nclimate2397.
Marzeion, B., A. H. Jarosch, M. Hofer, 2012: Past and future sea-level change from the surface mass balance of glaciers. *The Cryo*., **6**, 1295-1322, doi:10.5194/tc-6-1295-2012.
Menary, M. B., W. Park, K. Lohmann, M. Vellinga, M. D. Palmer, M. Latif, and J. H. Jungclaus, 2012: A multimodel comparison of centennial Atlantic meridional overturning circulation variability. *Climate Dyn.*, **38**, 2377–2388, doi:10.1007/s00382-011-1172-4.
Meyssignac, B., and A. Cazenave, 2012: Sea level: A review of present-day and recent-past changes and variability. *J. Geodyn.*, **58**, 96–109, doi:10.1016/j.jog.2012.03.005.
Meyssignac, B., X. Fettweis, R. Chevrier, and G. Spada, 2016: Regional sea level changes for the 20th and the 21st century induced by the regional variability in Greenland ice sheet surface mass loss. *J. Climate*, doi:10.1175/JCLI-D-16-0337.1.
Meyssignac, B, and Coauthors, 2017: Evaluating model simulations of Twentieth-Century sea-level rise. Part II: Regional sea-level changes. *J. Climate*, **30**, 8565–8593, doi:10.1175/JCLI-D-17-0112.1.
Msadek, R., W. E. Johns, S. G. Yeager, G. Danabasoglu, T. L. Delworth, and A. Rosati, 2013: The Atlantic meridional heat transport at 26.5°N and its relationship with the MOC in the RAPID Array and the GFDL and NCAR coupled models. *J. Climate*, **26**, 4335–4356, doi:10.1175/JCLI-D-12-00081.1.
Peltier, W. R., 2004: Global glacial isostasy and the surface of the ice-age earth: The ice-5G (VM2) model and grace. *Annu. Rev. Earth Planet. Sci.*, **32**, 111–149, doi:10.1146/annurev.earth.32.082503.144359.
Perrette, M., F. Landerer, R. Riva, K. Frieler, and M. Meinshausen, 2013: A scaling approach to project regional sea level rise and its uncertainties. *Earth Syst. Dyn.*, **4**, 11–29, doi:10.5194/esd-4-11-2013.Permanent Service for Mean Sea Level (PSMSL), 2016: Tide Gauge Data, Retrieved 16 April 2016 from http://www.psmsl.org/data/obtaining/.
Poli, P., and Coauthors, 2016: ERA-20C: An atmospheric reanalysis of the Twentieth Century. *J. Climate,* **29**, 4083–4097, doi:10.1175/JCLI-D-15-0556.1.
Power, S., M. Haylock, R. Colman, and X. Wang, 2006: The predictability of interdecadal changes in ENSO activity and ENSO teleconnections. *J. Climate*, **19**, 4755–4771, doi:10.1175/JCLI3868.1.
Ray, R. D., and B. C. Douglas, 2011: Experiments in reconstructing twentieth-century sea levels. *Prog. Oceanogr.*, **91**, 496–515, doi:10.1016/j.pocean.2011.07.021.
Schotman, H. H. A., 2008: Shallow-earth rheology from glacial isostasy and satellite gravity. PhD thesis, TU Delft, uuid:b3871b4b-247e-4344-91f6-bcff776e96c6.
Shepherd, A., and Coauthors, 2012: A reconciled estimate of ice-sheet mass balance. *Science*, **338**, 1183–1189, doi:10.1126/science.1228102.
Slangen, A. B. A., M. Carson, C. A. Katsman, R. S. W. van de Wal, A. Koehl, L. L. A. Vermeersen, and D. Stammer, 2014a: Projecting twenty-first century regional sea-level changes. *Climate Change*, **124**, 317–332, doi:10.1007/s10584-014-1080-9.
Slangen, A. B. A., R. S. W. van de Wal, Y. Wada, and L. L. A. Vermeersen, 2014b: Comparing tide gauge observations to regional patterns of sea-level change (1961–2003). *Earth Syst. Dyn.*, **5**, 243–255, doi:10.5194/esd-5-243-2014.
Slangen, A. B. A, J. A. Church, C. Agosta, X. Fettweis, B. Marzeion, and K. Richter, 2016: Anthropogenic forcing dominates global mean sea-level rise since 1970. *Nat. Climate Change*, **6**, 701–705, doi:10.1038/nclimate2991.
Slangen, A. B. A, and Coauthors, 2017: Evaluating model simulations of Twentieth-Century sea level rise. Part I: Global mean sea level change. *J. Climate*, **30**, 8539–8563, doi:10.1175/JCLI-D-17-0110.1.
Spada, G., and P. Stocchi, 2007: SELEN: A Fortran 90 program for solving the "sea-level equation." *Comput. Geosci.*, **33**, 538–562, doi:10.1016/j.cageo.2006.08.006.
Spada, G, J. L. Bamber, and R. T. W. L. Hurkmans, 2013: The gravitationally consistent sea-level fingerprint of future terrestrial ice loss. *Geophys. Res. Lett.*, **40**, 482–486, doi:10.1029/2012GL053000.
Taylor, K. E., R. J. Stouffer, and G. A. Meehl, 2012: An overview of CMIP5 and the experiment design. *Bull. Amer. Meteorol. Soc.*, **93**, 485–498, doi:10.1175/BAMS-D-11-00094.1.
Thompson, P. R., B. D. Hamlington, F. W. Landerer, and S. Adhikari, 2016: Are long tide gauge records in the wrong place to measure global mean sea level rise? *Geophys. Res. Lett.,* **43,** 10,403-10,411, doi:10.1002/2016GL070552.
Wada, Y., M.-H. Lo, P. J.-F. Yeh, J. T. Reager, J. S. Famiglietti, R.-J. Wu, and Y.-H. Tseng, 2016: Fate of water pumped from underground and contributions to sea-level rise. *Nat. Climate Change*, **6**, 777–780, doi:10.1038/nclimate3001.
Wöppelmann, G., C. Letetrel, A. Santamaria, M.-N. Bouin, X. Collilieux, Z. Altamimi, S. D. P. Williams, and B. M. Miguez, 2009: Rates of sea-level change over the past century in a geocentric reference frame. *Geophys. Res. Lett.*, **36,** doi:10.1029/2009GL038720.
Wunsch, C., and D. Stammer, 1997: Atmospheric loading and the oceanic "inverted barometer" effect. *Rev. Geophys.*, **35**, 79–107, doi:10.1029/96RG03037.

Changes in extreme sea levels

Marta Marcos[1,2] and Philip L. Woodworth[3]

[1]Mediterranean Institute for Advanced Studies, Spain
[2]University of the Balearic Islands, Spain
[3]National Oceanography Centre, UK

Changes in extreme sea levels are of great interest as one aspect of climate change and have a practical importance with regard to coastal protection. Extreme sea levels are the maximum levels of the sea that often occur during major storms and result in coastal flooding. Most of the evidence for changes in the frequency and magnitude of extreme sea levels has come from the worldwide network of tide gauges. These instruments have provided a quasi-global sea level dataset, with good coverage of the large parts of the global coastline since the mid-20th century (Woodworth et al. 2017).

The first study of changes in extreme sea levels on a global basis was that of Menéndez and Woodworth (2010). They concluded that the changes could be explained to a great extent by the underlying changes in mean sea level (MSL). In addition, they demonstrated a dependence of extreme sea levels on the main climate modes of variability, notably the El Niño Southern Oscillation (ENSO) and the North Atlantic Oscillation (NAO).

Other authors have confirmed these conclusions by looking into the reasons for changes in extreme sea levels at particular locations or in certain regions (e.g., Lowe et al. 2010; Woodworth et al. 2011; Seneviratne et al. 2012; Weisse et al. 2014). In a more recent study of the Bay of Bengal, Antony et al. (2016) also found changes in MSL to be an important driver of changes in extreme sea levels. It is important to note, however, that locations can be found where such a simple relationship does not apply.

North Atlantic extreme sea levels

The North Atlantic coastline has a relatively rich tide gauge dataset. Figure 1a shows trends in the 99th percentiles of measured sea levels in each year (i.e., the level that is equalled or exceeded during 88 of the 8760 hours in a normal year) from 1960 to present (Marcos and Woodworth 2017). High percentiles of sea level, such as 99 or 99.9%, are often used in studies of extremes, as they tend to be a more robust than the very highest (100%) values, which are sometimes lost due to equipment outages during the most violent events.

Most of Figure 1a is red, confirming anecdotal information from many countries that extreme sea levels have increased in recent years. An exception can be seen for the Baltic coasts of Finland and Sweden, where glacial isostatic adjustment contributes to a sea level fall. Trends are significantly different from zero at 70% of the stations on this map. When the annual MSL is removed from the observations (Figure 1b), most of the trends lose their significance. In other words, MSL change is a major contributor to the observed change in extreme sea level at these locations. However, significant linear changes are still present for about 23% of these locations, which

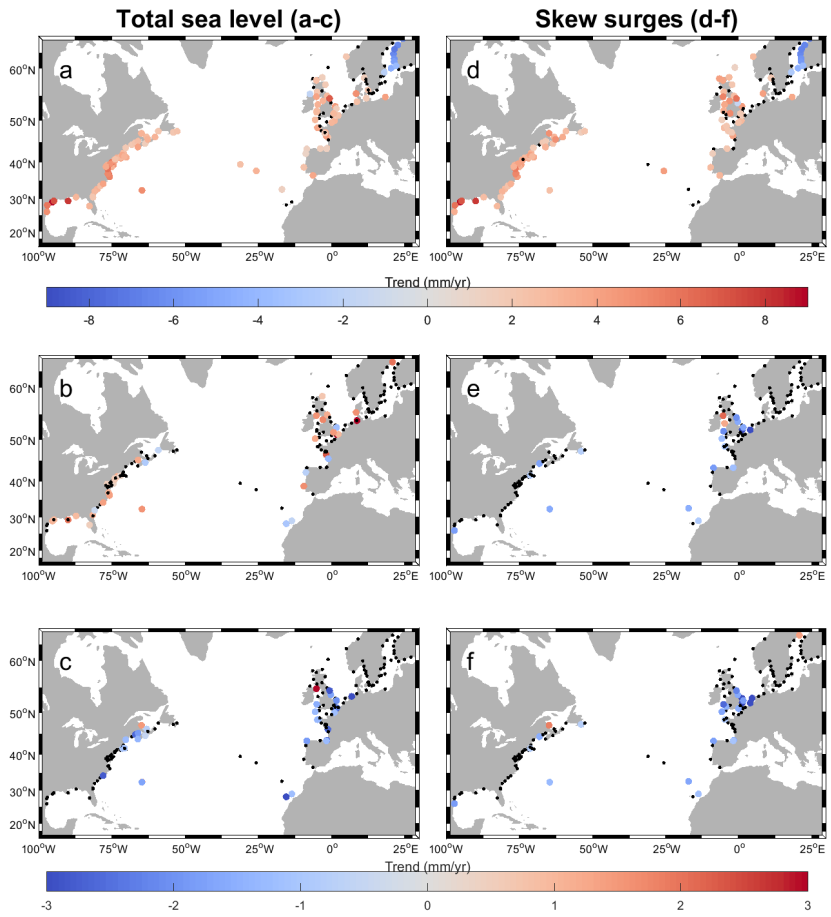

Figure 1. Linear trends (mm yr^{-1}) of annual 99th percentiles of a) total sea level, b) with median removed, and c) for non-tidal residuals with median removed. Linear trends of annual 99th percentiles of d) skew surges, e) with median removed, and f) with low-pass filter MSL removed. Tide gauge data from 1960 to present are used. Black dots indicate where the trends are not significant. (From Marcos and Woodworth 2017).

indicates that something other than MSL must also be responsible. Figure 1c provides a similar conclusion to Figure 1b but uses what are called non-tidal residuals (NTRs) instead of the measured levels. NTRs are time series of sea levels for which the astronomical ocean tide has been removed from the total measured levels (Figure 2). The number of stations with significant trends remains similar, although the actual trend values change at most sites. Overall, these results are in agreement with Menéndez and Woodworth (2010) in terms of the sign of the linear trends and the reduction of the significant stations when MSL variations are subtracted from the observations.

An alternative to NTRs is the use of skew surges (de Vries et al. 1995; Pugh and Woodworth 2014; Williams et al. 2016). These are the differences between the observed maximum water heights and the predicted tidal high-water levels within each tidal cycle (Figure 2). They have advantages over NTRs in being a more robust parameter for studying extremes when using tide gauge data with poor timing. Poor timing, as a result of errors in tide gauge clocks, is often found in historical data and results in a distortion of the computed NTRs. In addition, the skew surge represents the extent to which a tidal prediction is exceeded during a storm event, which is what coastal engineers want to know. If the astronomical tide used in the computation of the skew surge does not include MSL, then any variation in MSL (interannual variability or long-term trends) will manifest itself in the skew surge values.

We have investigated temporal changes in skew surges in a similar way to total sea levels and NTRs. The spatial patterns of trends in skew surges (Figure 1d) follow, once again, the linear trends in MSL and are very similar to those obtained for total sea level (Figure 1a). Approximately 65% of stations in the map have trends significantly different from zero in the 99th percentile of skew surges each year, which reduces to ~10% when the median skew surge for the year is removed from each individual value (Figure 1e). Figure 1f provides similar information but using a low-pass filtered estimate of

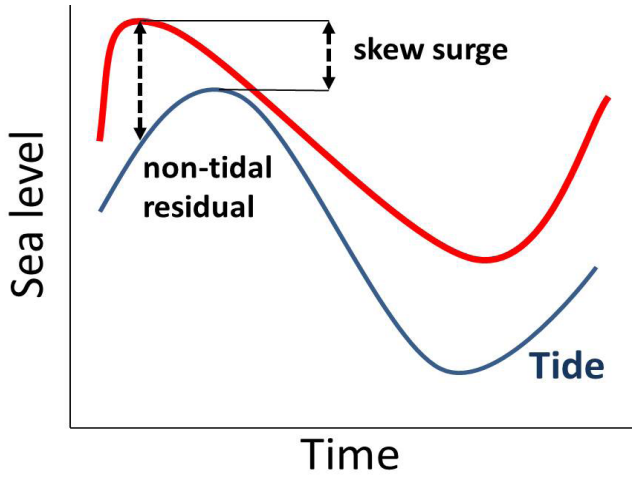

Figure 2. Schematic explanation of non-tidal residual (NTR) and skew surge during one semi-diurnal cycle.

MSL instead of the annual mean. The comparison of Figure 1(a-c) with (d-f) confirms that the high percentiles of total sea level and skew surges present the same behaviour in terms of spatial patterns and trends, in line with earlier works (e.g., Dangendorf et al. 2014; Mawdsley and Haigh 2016). Similar conclusions are obtained when either NTRs or skew surges are studied on a seasonal, rather than annual, basis.

Figure 3a shows correlations of the 99th percentiles of skew surges during each year and the NAO index, using the 1960 to present record. High positive correlations can be seen in the eastern North Sea and Baltic regions, with negative correlations at some locations along the North American coastline. The high positive correlations for the North Sea and Baltic are related to the strong westerly winds associated with a high NAO index. The same winds also produce a positive correlation of MSL and NAO index in Northern Europe (e.g., Andersson 2002; Wakelin et al. 2003). Nevertheless, MSL variability cannot account for all the changes in extreme sea levels, and, if MSL is removed, the pattern of correlations remains much the same, if somewhat weaker (Figure 3b), indicating that the influence of the NAO is not only limited to the MSL (see also Woodworth and Blackman 2004).

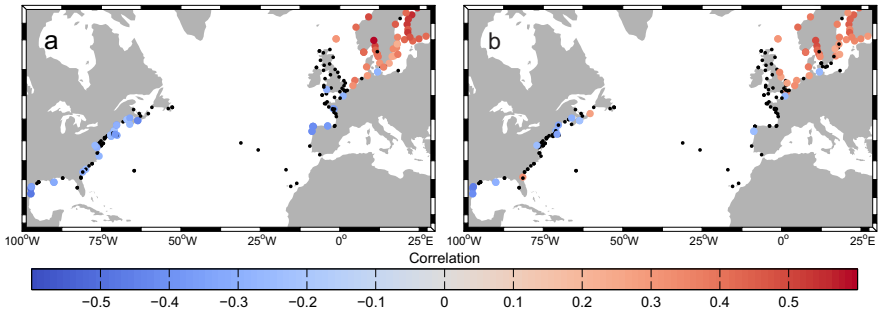

Figure 3. Correlations between the 99th percentiles of skew surges and the NAO a) without and b) with MSL removed from the skew surge values. (From Marcos and Woodworth 2017).

Links with large-scale climate indices

Variability in extreme sea levels on interannual and decadal timescales has been related to large-scale climate modes by a number of authors (Marcos et al. 2009; Menéndez and Woodworth 2010; Talke et al. 2014; Marcos et al. 2015; Mawsdley and Haigh 2016; Wahl and Chambers 2016). In many regions, such as along Pacific coasts, extreme sea levels associated with ENSO result, to a great extent, from changes in MSL (Menéndez and Woodworth, 2010). However, Marcos and Woodworth (2017) provide an example where there is more to extreme sea levels than MSL.

Extreme sea level distributions

Coastal engineers and managers need good information of the probability of extreme events in order to design structures and strategies, as well as calculate the costs of the impacts of flooding, should defenses fail in the future as sea level rises (Hunter et al. 2017). Engineers parameterise the probability of extreme sea levels at a particular location in terms of a generalized extreme level (GEV) distribution, comprising three parameters: location, scale, and shape (Coles 2001; Menéndez and Woodworth 2010). In many cases, a restricted Gumbel distribution is employed, in which the shape parameter is set to zero.

We have investigated the possible deficiencies in using the simple Gumbel approach using records from around the North Atlantic coastline, assuming stationarity in location, scale, and shape parameters (Marcos and Woodworth 2017). Only records with at least 25 years of valid data since 1960 were used. We found that only in ~27% of the stations is the Gumbel fit to be considered adequate (and preferred for simplicity) compared to the GEV parameterization. These stations are distributed primarily in the North Sea and along the North American coast. At most stations, where a GEV is preferred, the shape parameter is mostly negative but ranges between -0.3 and 0.3 (Figure 4). Largest negative values are located along the Atlantic European coasts, while there are positive values in the Canary Islands, the Gulf of Mexico, and at low latitudes along the North American coast. The geographical coherence provides confidence in the obtained values. The shape parameter has highest positive values in the Gulf of Mexico during summer, consistent with extreme sea levels in this region being dominated by tropical cyclones at that time (Tebaldi et al. 2012). Individual positive shape parameters may arise as an artifact of inadequate sampling of the rare events from tropical cyclones. Negative shape parameters are found in most parts of the world outside the tropics, an observation, which needs to be taken into account in coastal engineering and impact studies. Negative shapes at most sites around the world were also obtained in a study by Wahl et al. (2017) and the reasons for them are presently being explored in more detail.

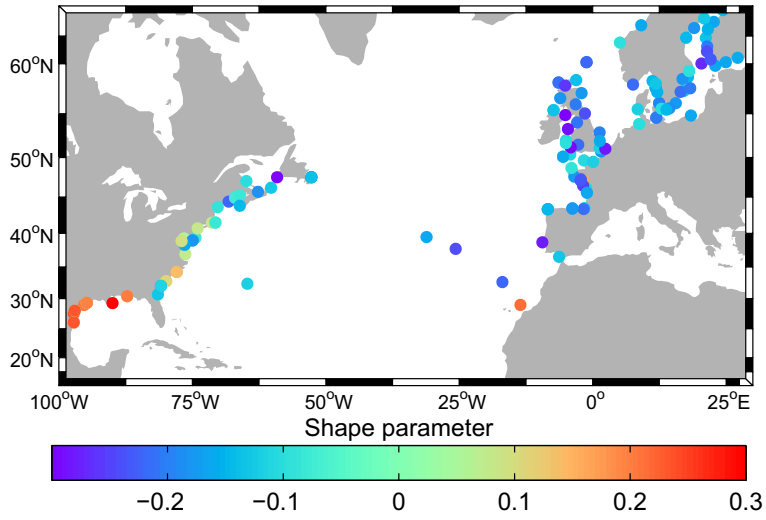

Figure 4. Shape parameters obtained from GEV fits to annual extreme sea levels (after removing MSL) at locations where a GEV distribution provides a superior fit to a Gumbel description in which the shape parameter is set to zero. (From Marcos and Woodworth 2017).

Conclusions

Many authors have recognised the importance of changes in MSL to changes in the occurrence of extreme sea levels. For example, in regards to the US Atlantic coast, Zhang et al. (2010) were among the first to point out the similarity in time series of both MSL and extreme sea levels. These are important findings with regard to designing coastal defenses for the future (Hunter 2012). The prediction of future changes in MSL is already difficult (Church et al. 2013), and designing defenses for the future would be even harder if extreme sea levels were to change independently of mean sea level.

However, versions of Figure 3 with and without MSL removed demonstrate that MSL is not the whole story. Using the US coast as an example again, Wahl and Chambers (2015) also demonstrated the importance of MSL to extreme sea levels but also pointed to sections of coast where additional (non-MSL) processes were important.

We suggest two areas of work that might lead to further understanding of extreme sea levels. The first is more high-resolution climate modeling and understanding of the links between extreme sea levels, ENSO, NAO, and Atlantic Multidecadal Oscillation that have been identified on both sides of the North Atlantic (see Marcos and Woodworth 2017 for recent references). The second is the need for the 'data archaeology' of longer records

of MSL and extreme sea levels from locations where tide gauges have been operated for many years but the records have not been made available for research. New York (Talke et al. 2014) is a good example, with an available record now extending back to 1844. More records such as this would help us better understand the extreme sea levels of the past and provide insight into estimating extremes in the future.

References

Andersson, H. C., 2002: Influence of long-term regional and large-scale atmospheric circulation on the Baltic sea level. *Tellus,* **54A,** 74-88, doi:10.1034/j.1600-0870.2002.00288.x.

Antony, C., A. S. Unnikrishnan, and P. L. Woodworth, 2016: Evolution of extreme high waters along the east coast of India and at the head of the Bay of Bengal. *Glob. Planet. Change,* **140,** 59-67, doi:10.1016/j.gloplacha.2016.03.008.

Church, J. A., and Coauthors, 2013: Sea Level Change. *Climate Change 2013: The Physical Science Basis. Contribution of Working Group I to the Fifth Assessment Report of the Intergovernmental Panel on Climate Change*. Stocker, T. F., D. Qin, G.-K. Plattner, M. Tignor, S. K. Allen, J. Boschung, A. Nauels, Y. Xia, V. Bex and P. M. Midgley, Eds., Cambridge University Press, Cambridge, UK and New York, NY, USA, doi:10.1017/CBO9781107415324.026.

Coles, S., 2001: An introduction to statistical modeling of extreme values. Springer, London, UK, 224pp., doi:10.1007/978-1-4471-3675-0.

Dangendorf, S., S. Muller-Navarra, J. Jensen, F. Schenk, T. Wahl, and R. Weisse, 2014: North Sea storminess from a novel storm surge record since AD 1843. *J. Climate,* **27,** 3582–3595, doi:10.1175/JCLI-D-13-00427.1.

de Vries, H., and Coauthors, 1995: A comparison of 2D storm surge models applied to three shallow European seas. *Environ. Softw.,* **10,** 23–42, doi:10.1016/0266-9838(95)00003-4.

Hunter, J., 2012: A simple technique for estimating an allowance for uncertain sea-level rise. *Climatic Change,* **113,** 239–252, doi:10.1007/s10584-011-0332-1.

Hunter, J. R., P. L. Woodworth, T. Wahl, and R. J. Nicolls, 2017: Using global tide gauge data to validate and improve the representation of extreme sea levels in flood impact studies. *Glob. Planet. Change,* **156,** 34-45, doi:10.1016/j.gloplacha.2017.06.007.

Lowe, J. A., and Coauthors, 2010: Past and future changes in extreme sea levels and waves. *Understanding sea-level rise and variabili*ty, J. A. Church, P.L. Woodworth, T. Aarup, and W. S. Wilson, Eds.. Wiley-Blackwell, London, UK, doi:10.1002/9781444323276.ch11

Marcos, M., M. N. Tsimplis, and A. G. P. Shaw, 2009: Sea level extremes in southern Europe. *J. Geophys. Res.,* **114***,* doi:10.1029/2008JC004912.

Marcos, M., F. M. Calafat, A. Berihuete, and S. Dangendorf, 2015: Long-term variations in global sea level extremes. *J. Geophys. Res. Oceans,* **120,** 8115-8134, doi:10.1002/2015JC011173.

Marcos, M., and P. L. Woodworth, 2017: Spatio-temporal changes in extreme sea levels along the coasts of the North Atlantic and the Gulf of Mexico. *J. Geophys. Res. Oceans,* **122,** 7031-7048, doi:10.1002/2017JC013065.

Mawdsley, R. J., and I. D. Haigh, 2016: Spatial and temporal variability and long-term trends in skew surges globally. *Front. Mar. Sci.,* **3,** doi:10.3389/fmars.2016.00029.

Menéndez, M., and P. L. Woodworth, 2010: Changes in extreme high water levels based on a quasi-global tide-gauge dataset. *J. Geophys. Res.,* **115,** doi:10.1029/2009JC005997.

Pugh, D. T., and P. L. Woodworth, 2014: Sea-level science: Understanding tides, surges, tsunamis and mean sea-level changes. Cambridge University Press, UK, 408pp., ISBN:9781107028197.

Seneviratne, S. I., and Coauthors, 2012: Changes in climate extremes and their impacts on the natural physical environment. *Managing the Risks of Extreme Events and Disasters to Advance Climate Change Adaptation,* Field, C.B., V. Barros, T.F. Stocker, D. Qin, D.J. Dokken, K.L. Ebi, M.D. Mastrandrea, K.J. Mach, G.-K. Plattner, S.K. Allen, M. Tignor, and P.M. Midgley, Eds., A Special Report of Working Groups I and II of the Intergovernmental Panel on Climate Change (IPCC). Cambridge University Press, Cambridge, UK, and New York, NY, USA, pp. 109-230, https://www.ipcc.ch/pdf/special-reports/srex/SREX-Chap3_FINAL.pdf.

Talke, S. A., P. Orton, and D. A. Jay, 2014: Increasing storm tides in New York Harbor, 1844-2013. *Geophys. Res. Lett.,* **41,** 3149-3155, doi:10.1002/2014GL059574.

Tebaldi, C., B. H. Strauss, and C. E. Zervas, 2012: Modelling sea level rise impacts on storm surges along US coasts. *Env. Res. Lett.,* **7,** doi:10.1088/1748-9326/7/1/014032.

Wahl, T., and D. P. Chambers, 2015: Evidence for multidecadal variability in US extreme sea level records. *J. Geophys. Res. Oceans,* **120,** 1527-1544, doi:10.1002/2014JC010443.

Wahl, T., and D. P. Chambers, 2016: Climate controls multidecadal variability in U. S. extreme sea level records. *J. Geophys. Res. Oceans,* **121,** 1274-1290, doi:10.1002/2015JC011057.

Wahl, T., I. D. Haigh, R. J. Nicholls, A. Arns, S. Dangendorf, J. Hinkel, and A. B. A. Slangen, 2017: Understanding extreme sea levels for broad-scale coastal impact and adaptation analysis. *Nat. Comm.,* **8,** doi:10.1038/ncomms16075.OI: 10.1038/ncomms16075.

Wakelin, S. L., P. L. Woodworth, R. A. Flather, and J. A. Williams, 2003: Sea-level dependence on the NAO over the NW European Continental Shelf. *Geophys. Res. Lett.,* **30,** doi:10.1029/2003GL017041.

Weisse, R., D. Bellafiore, M. Menéndez, F. Méndez, R. J. Nicholls, G. Umgiesser, and P. Willems, 2014: Changing extreme sea levels along European coasts. *Coast. Eng.,* **87,** 4-14, doi:10.1016/j.coastaleng.2013.10.017.

Williams, J., K. J. Horsburgh, J. A. Williams, and R. N. F. Proctor, 2016: Tide and skew surge independence: New insights for flood risk. *Geophys. Res. Lett.,* **43,** 6410-6417, doi:10.1002/2016GL069522.

Woodworth. P. L., and D. L. Blackman, 2004: Evidence for systematic changes in extreme high waters since the mid-1970s. *J. Climate,* **17,** 1190-1197, doi:10.1175/1520-0442.

Woodworth, P. L., M. Menéndez, and W. R. Gehrels, 2011: Evidence for century-timescale acceleration in mean sea levels and for recent changes in extreme sea levels. *Surv. Geophys.,* **32,** 603-618, doi:10.1007/s10712-011-9112-8.

Woodworth, P. L., J. R. Hunter, M. Marcos, P. Caldwell, M. Menéndez, and I. Haigh, 2017: Towards a global higher-frequency sea level data set. *Geosci. Data J.,* **3,** 50-59, doi:10.1002/gdj3.42.

Zhang, K. Q., B. C. Douglas, and S. P. Leatherman, 2000: Twentieth-century storm activity along the US east coast. *J.Climate,* **13,** 1748-1761, doi:10.1175/1520-0442(2000)013<1748:TCSAAT>2.0.CO;2.

ENSO teleconnections across the Pacific

Justin E. Stopa[1] and Mark Merrifield[2]

[1]LOPS, University of Brest, CNRS, IRD, Ifremer, France
[2]Scripps Institution of Oceanography, US

Regional sea level is influenced by thermal expansion and melting ice sheets (Rahmstorf et al. 2007; Rignot et al. 2011), land subsidence (Wang et al. 2012), seasonal/annual astronomical tides, and non-tidal residuals, which include sea level anomalies such as storm surge, wind setup, and wave setup (Merrifield et al. 2012). Sea level is expected to rise, and this puts coastal communities at risk from high water levels (Sweet and Park 2014). The effects of wave-driven sea level anomalies are often not considered to impact regional sea levels. However, it is has been reported that wave-driven anomalies cause inundation especially in episodic events (Lefevre 2008; Hoeke et al. 2013). Therefore, low-lying regions of the Pacific can be vulnerable to swells, since they persist for days ensuring the coincidence of a high tide. In this work, we focus on exploring the relationship between El Niño Southern Oscillation (ENSO), the wave field in the North Pacific's winter, and sea level anomalies.

ENSO has a strong interannual variability signal having far-reaching effects on the global weather and climate patterns. ENSO modifies rainfall patterns (Ropelewski and Halpert 1987; Wang et al. 2000), ocean-atmosphere temperatures (Klein et al. 1999), and atmospheric pressure (Fraedrich and Mueller 1992). In the North Pacific winter (December-January-February, DJF), there is a notable change in the pressure anomalies, which influence the wave field (Graham and Diaz 2001; Menendez et al. 2008; Stopa and Cheung 2014a). The ENSO ocean wave interannual variability affects beach profiles (such as erosion and flooding) across the Pacific (Allan and Komar 2006; Barnard et al. 2011, 2015) and creates sea level anomalies in the western Pacific (Merrifield et al. 2012). Yet the relationship between the atmospheric forcing, expected change in storm tracks, and wave field is not well established. In this work, we explore the teleconnection between ENSO, through the change in storm tracks, and the effect on sea level anomalies, through swells in the far-field.

Approach

Using wave data generated by a wave hindcast from the NOAA National Center for Environmental Prediction (NCEP) climate forecast system reanalysis (CFSR), we examine wave heights throughout the Pacific region. Typically wave hindcasts are not consistent in time, due to the fact that the quality and quantities of the satellite data assimilated into the product change with time (Stopa and Cheung 2014b). Therefore, we made efforts to ensure our data is consistent in time using a merged multi-mission satellite altimeter database as reference (Queffeulou and Croize-Fillon 2015). To remove longer term variability, the forcing wind field is modified by a small percentage (1-5%) each month in the Northern and Southern Hemispheres to produce a homogeneous time series. Figure 1 shows the wave height before and after the correction. In the figure, we are showing the 95th

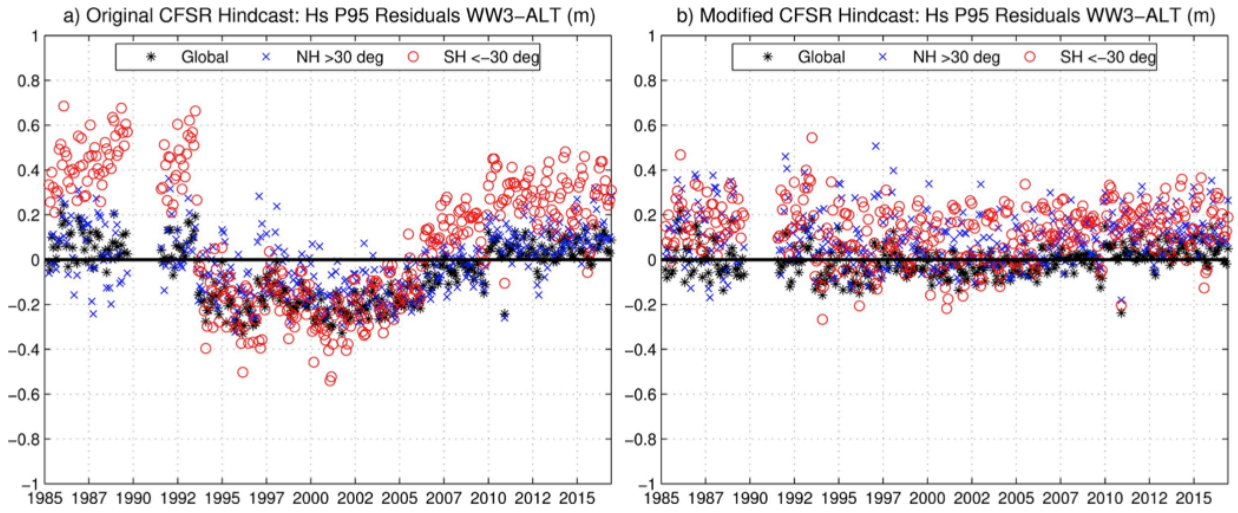

Figure 1. Significant wave height (Hs) monthly residuals (model-altimeter) computed for each region (black stars: global; blue crosses: Northern Hemisphere; red circles: Southern Hemisphere) for the 95th percentile (P95) for a wave hindcast using the CFSR. Results are the a) original hindcast and b) after the winds are empirically scaled to reduce the P95 Hs residual.

percentile, since it is more sensitive to changes in the data compared to the mean. We see seasonality (amplitude of 40 cm) of the residuals, which might be related to errors of the spectral wave model or errors in the altimeter data. The wave hindcast uses physical parameterizations from Ardhuin et al. (2010) and covers 1979–2016 globally (Stopa and Ardhuin 2017).

We focus our efforts on the winter months in the North Pacific (140-240ºE, 25-60ºN) and track storms in the wave field. We follow similar methodology as tracking storms in the atmosphere (Hoskins and Hodges 2002). We track the strong and persistent storms that have a significant wave height (Hs) that at least exceeds 6 m and is active for at least 24 hours. Our method captures the strongest extra-tropical events, but short-lived compact storms are not analyzed. Once each storm is tracked, we find the maximum wave height and use this as a proxy for the storm strength.

The tide gage data, from a several stations from the University of Hawai'i Sea Level Center, are analyzed. Our aim is to match the arrival times of the swells associated with the tracked storms to sea level anomalies. The sea level anomalies were created by removing the effects from regional sea level.

Results

Example years from the stronger El Niño (1998) and La Niña (1989), and neutral (1982) events — based on the Oceanic Nino Index (ONI) as defined by Huang et al. (2017) (+2.2, -1.7, 0.0 respectively) — are taken as representative years from the 37-year hindcast. The storm tracks are plotted in Figure 2. The color represents the maximum storm wave height. From these examples, it is clear that during neutral and La Niña years the intensity of the storms are comparable, while during El Niño years the strength of the storms increases. During the 1998 El Niño, nine storms exceed the maximum wave height of 11 m, while only three storms breach this threshold for both neutral and La Niña years. The 1998 El Niño was particularly active, with 42 storms, as compared to the other strong El Niño years (where ONI>2) (e.g., 1983 and 2016). However, we found, on average, the number of large storms during El Niño were comparable to La Niña

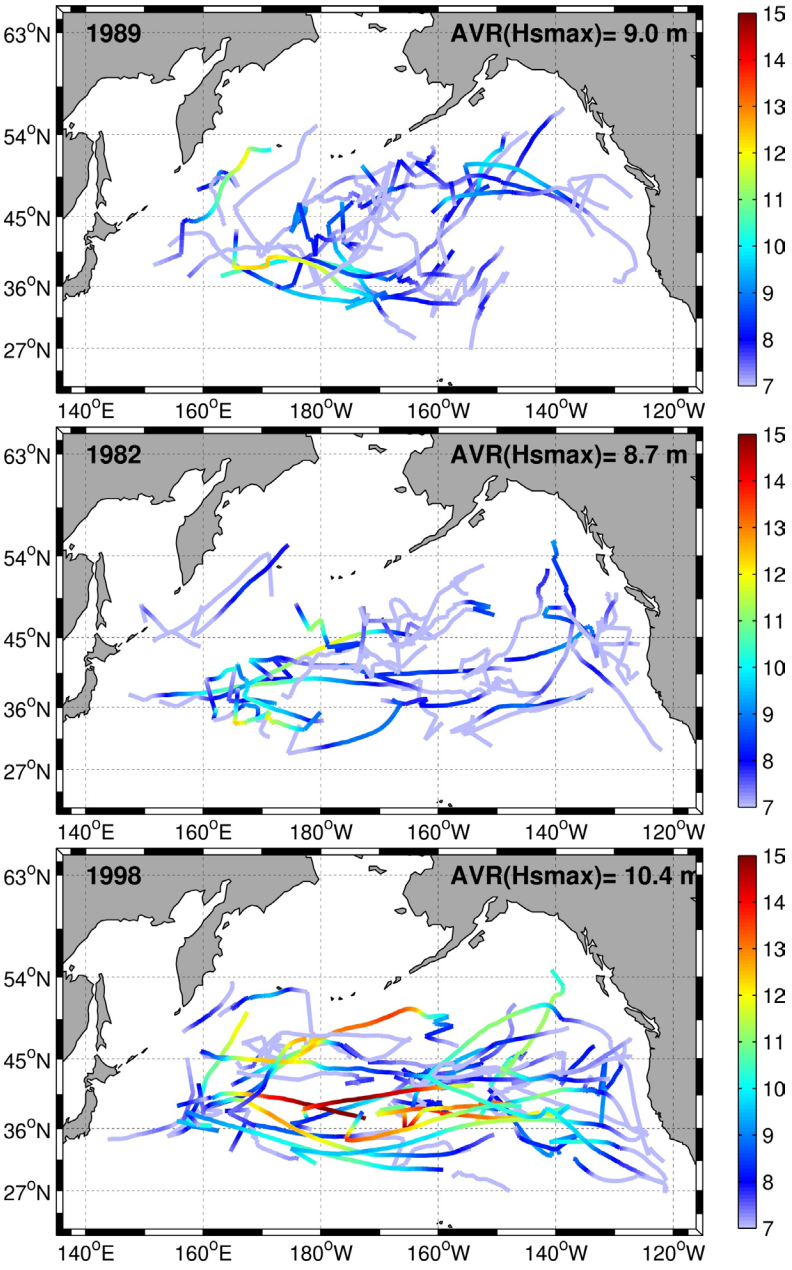

Figure 2. Storm tracks for representative years of La Niña (1989, top), neutral (1982, middle), and El Niño (1998, bottom), color coded by the significant wave height (m).

and neutral years. In total, the three strongest El Niño (1998, 2016, 1983), La Niña (1989, 2000, 2008), and neutral (1982, 1990, 1994) years have 88, 90, and 102 storms respectively.

Using the tracked storms, we propagate the swells into the far field and analyze the sea level anomalies. Several tide gauges inside Pacific atolls respond to oceanic swells due to the wave setup that is produced inside the lagoon Aucan et al. (2012). To demonstrate the impact of swells on the tide gages, we show one example storm in the North Pacific that occurred February 11–16, 1998. The storm took a westerly track and propagated below 40°N. Three daily averages of the wave energy flux are given in Figure 3 (left). The corresponding sea level anomalies and wave power time series are given in Figure 3 (right). At Midway Atoll on February 11 (Figure 3a), it is clear that the wave-induced setup is indeed creating the high sea level anomalies. Two days later on February 13 (Figure 3b), the peak energy of the storm propagated to Johnston Atoll, and the increased wave energy corresponds with a positive sea level anomaly. In far-field at Cook Islands (Penrhyn tide gage) on February 15, the increased wave energy corresponds to a positive sea level anomaly. Note that the ordinate axes are different in each time series plot. At Penrhyn, the sea level anomalie is only 10 cm and it is not clear whether this magnitude would in fact cause inundation.

What is important here is that this example demonstrates the coherency of the wave event across the Pacific. And more importantly, the increased wave energy coincides with positive sea level anomalies. At all of these tide gages, the correlation was strong and exceeds 0.7. Along the West Coast of North America, it was observed that several tide gauges respond

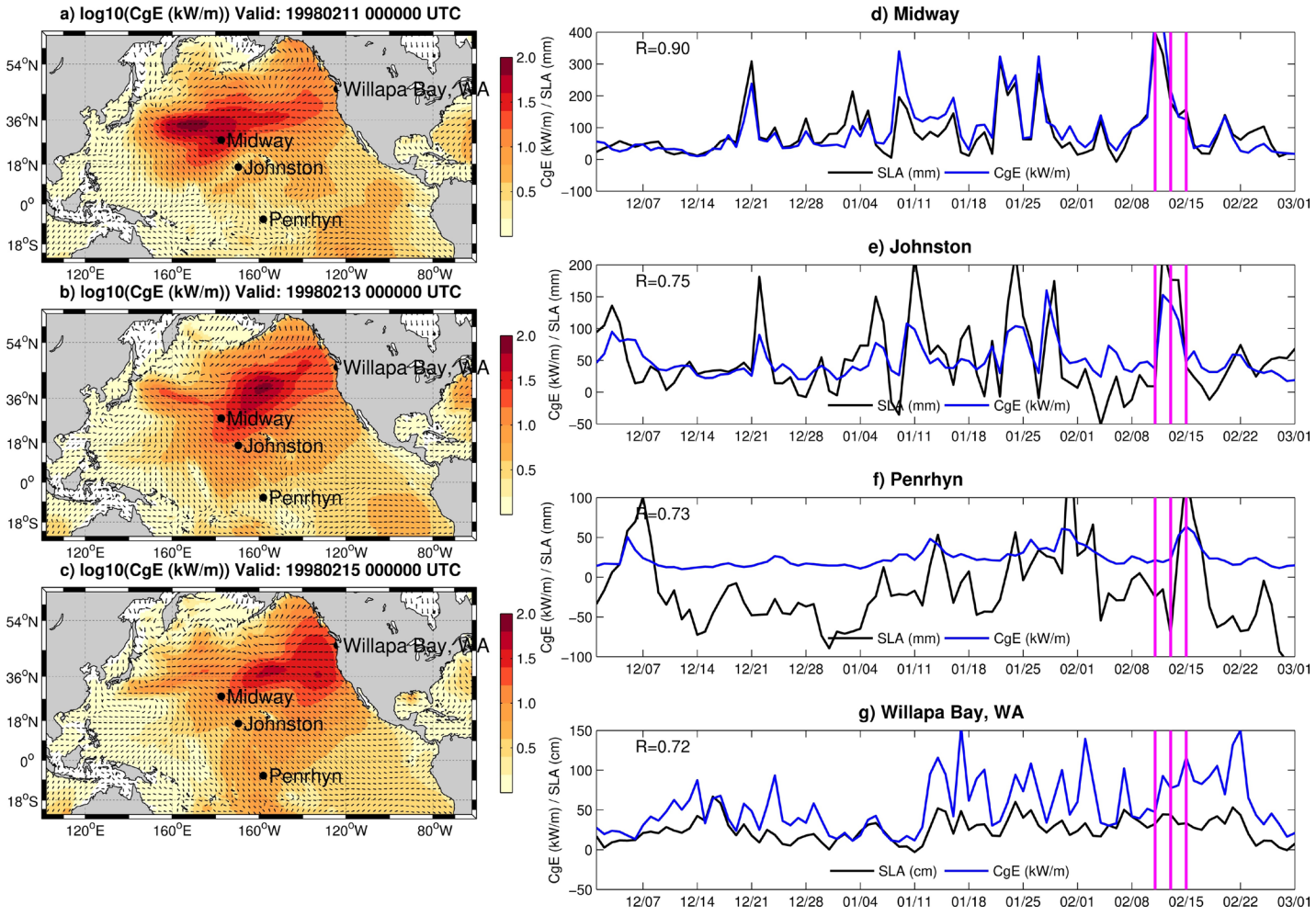

Figure 3. Example storm in the North Pacific (a,b,c), where the color bar represents the wave power and the arrows represent the wave direction. The wave power is given on a logarithmic scale. Panels d-g show the sea level anomalies and wave energy for four tide gages across the Pacific (Midway, Johnston, Penrhyn, and Willapa Bay). The vertical magenta lines correspond to a, b, and c, respectively, and represents the wave power. The correlation coefficient (R) between the wave power and sea level anomalies is given in each panel.

to wave events as well, as seen at Willapa Bay station in Washington. On February 15, as the remnants of the storm approaches, there is a small positive sea level anomaly that appears to be associated with the event. The time series reveal other events that are also consistent across the Pacific (e.g., January 10–16 and 26–31). In short, we find that these larger magnitude storms often coincide with significant positive sea level anomalies at tide gauges across the Pacific.

Conclusion and outlook

We find notable differences in the statistics of tracked storms in the wave field in the North Pacific's winter relative to ENSO phase. In particular, during El Niño years, the events are often strengthened compared to neutral and La Niña years, confirming other studies (Menendez et al. 2008; Bromirski et al. 2013). We find only a subtle difference in the number of events per year: El Niño years average 34 storms per season, while

La Niña and neutral years average 30 storms per season. Previous studies (e.g., Graham and Diaz 2001; Menendez et al. 2008; Bromirski et al. 2013) demonstrated that during El Niño years, the US West Coast wave action is elevated, agreeing with our results that the magnitude of the storms changes relative to the ENSO phase. We also observed that the storm tracks change relative to the ENSO phase, suggesting the far-field swell pattern is also modified during the respective years. Looking to the future, we are analyzing far-field effects through tracking the individual storms. The analysis of particular wave events, as shown in Figure 3, is certainly convincing that the positive sea level anomalies often coincide with energetic sea states. By using daily tide records, we find that the signal is persistent. Therefore, wave interannual variability could have some effect on trends when short time periods (less than 25 years) are used.

References

Ablain, A., and Coauthors, 2015: Improved sea level record over the satellite altimetry era (1993–2010) from the Climate Change Initiative project. *Ocean Sci.,* **11**, 67-82, doi:10.5194/os-11-67-2015.

Allan, J. C., and P. D. Komar, 2006: Climate controls on US West Coast erosion processes. *J. Coast. Res*. **223**, 511–529, doi:10.2112/03-0108.1.

Ardhuin, F. and Coauthors, 2010: Semiempirical dissipation source functions for ocean waves. part i: Definition, calibration, and validation. *J. Phys. Oceanogr*. **40**, 1917–1941, doi: 10.1175/2010JPO4324.1.

Aucan, J., R. Hoeke, and M. A. Merrifield, 2012: Wave-driven sea level anomalies at the Midway tide gauge as an index of North Pacific storminess over the past 60 years. *Geophys. Res. Lett*., **39**, , doi:10.1029/2012GL052993.

Barnard, P. L., J. Allan, J. E. Hansen, G. M. Kaminsky, P. Ruggiero, and A. Doria, 2011: The impact of the 2009-10 El Nino modoki on U.S. west coast beaches. *Geophys. Res. Lett.* **38**, doi:10.1029/2011gl047707.

Barnard, P. L., and Coauthors, 2015: Coastal vulnerability across the pacific dominated by El Nino/ Southern Oscillation. *Nat. Geosci*. **8**, 801–807, doi:10.1038/ngeo2539.

Bromirski, P. D., D. R. Cayan, J. Helly, and P. Wittmann, 2013: Wave power variability and trends across the north pacific. *J. Geophys. Res. Ocean*. **118**, 6329–6348, doi:10.1002/2013jc009189.

Graham, N. E. and H. F. Diaz, 2001: Evidence for intensification of north pacific winter cyclones since 1948. *Bull. Amer. Meteorol. Soc*. **82**, 1869–1893, doi:10.1175/1520-0477(2001)082¡1869:efionp¿2.3.co;2.

Hoeke, R. K., K. McInnes, J. C. Kruger, R. J. McNaught, J. R. Hunter, and S. G. Smithers, 2013: Widespread inundation of pacific islands triggered by distant-source wind-waves. *Glob. Planet. Change,* **108**, 128–138, doi:10.1016/j.gloplacha.2013.06.006.

Hoskins, B. J. and K. I. Hodges, 2002: New perspectives on the northern hemisphere winter storm tracks. *J. Atmos. Sci*., **59**, 1041–1061, doi:10.1175/1520-0469(2002)059¡1041:npotnh¿2.0.co;2.

Huang, B., P.W. Thorne, V.F. Banzon, T. Boyer, G. Chepurin, J.H. Lawrimore, M.J. Menne, T.M. Smith, R.S. Vose, and H. Zhang, 2017: Extended Reconstructed Sea Surface Temperature, Version 5 (ERSSTv5): Upgrades, Validations, and Intercomparisons. *J. Climate,* **30**, 8179–8205, https://doi.org/10.1175/JCLI-D-16-0836.1.

Lefevre, J.-M., 2008: High swell warnings in the Caribbean islands during march 2008. *Nat. Haz.,* **49**, 361–370, doi:10.1007/s11069-008-9323-6.

Menendez, M., F. J. Mendez, I. J. Losada, and N .E. Graham, 2008: Variability of extreme wave heights in the northeast Pacific Ocean based on buoy measurements. *Geophys. Res. Lett.* **35**, doi:10.1029/2008gl035394.

Merrifield, M. A., P. R. Thompson, and M. Lander, 2012: Multidecadal sea level anomalies and trends in the western tropical Pacific. *Geophys. Res. Lett.,* 39, doi:10.1029/2012gl052032.

Queffeulou, P. and D. Croize-Fillon, 2015: Global altimeter swh data set. Technical Report 11.1, IFREMER/CERSAT, ftp://ftp.ifremer.fr/ifremer/cersat/products/swath/altimeters/waves/documentation/.

Rahmstorf, S., 2007: A semi-empirical approach to projecting future sea-level rise. *Science,* **315**, 368–370 doi:10.1126/science.1135456.

Rascle, N. and F. Ardhuin, 2013: A global wave parameter database for geophysical applications. part 2: Model validation with improved source term parameterization. *Ocean. Model.,* **70**, 174–188, doi:110.1016/j.ocemod.2012.12.001.

Rignot, E., I. Velicogna, M. R. van den Broeke, A. Monaghan, and J. T. M. Lenaerts, 2011: Acceleration of the contribution of the greenland and antarctic ice sheets to sea level rise. *Geophys. Res. Lett*. **38**, doi:10.1029/2011gl046583.

Ropelewski, C. F. and M. S. Halpert, 1987: Global and regional scale precipitation patterns associated with the el niño/southern oscillation. *Mon. Wea. Rev*., **115**, 1606–1626, doi:10.1175/1520-0493(1987)115¡1606:garspp¿2.0.co;2.

Saha, S. and Coauthors, 2010: The NCEP climate forecast system reanalysis. *Bull. Amer. Meteorol. Soc*., **91**, 1015–1057, doi:10.1175/2010bams3001.1.

Stopa, J. E. and F. Ardhuin, 2017: A consistent wave hindcast using NCEP's Climate Forecast System Reanalysis. 14th Workshop on Wave Hindcasting and Forecasting, Liverpool, UK (11-15 September).

Stopa, J. E. and K. F. Cheung, 2014a: Periodicity and patterns of ocean wind and wave climate. *J. Geophys. Res. Ocean.* **119**, 5563–5584, doi:10.1002/2013jc009729.

Stopa, J. E. and K. F. Cheung, 2014b: Intercomparison of wind and wave data from the ECMWF reanalysis interim and the NCEP climate forecast system reanalysis. *Ocean. Model,*. **75**, 65–83, doi:10.1016/j.ocemod.2013.12.006.

Sweet, W. V. and J. Park, 2014: From the extreme to the mean: Acceleration and tipping points of coastal inundation from sea level rise. *Earth's Future*, **2**, 579–600, doi:10.1002/2014ef000272.

Wang, B., R. Wu, and X. Fu, 2000: Pacific-east Asian teleconnection: How does ENSO affect east Asian climate? *J. Climate,* **13**, 1517–1536, doi:10.1175/1520-0442(2000)013¡1517:peathd¿2.0.co;2.

Wang, J., W. Gao, S. Xu, and L. Yu, 2012: Evaluation of the combined risk of sea level rise, land subsidence, and storm surges on the coastal areas of Shanghai, China. *Climate Change*, **115**, 537–558, doi:10.1007/s10584-012-0468-7.

New York City's evolving flood risk from hurricanes and sea level rise

Andra J. Garner[1], Robert E. Kopp[1], Benjamin P. Horton[1,2], Michael E. Mann[3], Richard B. Alley[3], Kerry A. Emanuel[4], Ning Lin[5], Jeffrey P. Donnelly[6], Andrew C. Kemp[7], Robert M. DeConto[8], David Pollard[3]

[1]Rutgers University, US
[2]Nanyang Technological University, Singapore
[3]The Pennsylvania State University, US
[4]Massachusetts Institute of Technology, US
[5]Princeton University, US
[6]Woods Hole Oceanographic Institution, US
[7]Tufts University, US
[8]University of Massachusetts Amherst, US

On the evening of October 29th, 2012, Hurricane Sandy made landfall along the mid-Atlantic coast, bringing with it strong winds, destructive waves, and a catastrophic storm surge in New York Harbor. Hurricane Sandy generated a storm surge height of 2.87 m above mean tidal level (MTL) at The Battery in New York City (NYC) (Blake et al. 2013). The storm destroyed more than 650,000 buildings, 8 million customers lost power, and roads, bridges, and subways were closed, mainly as a result of the enormous storm surge and large waves (Blake et al. 2013). Hurricane Sandy highlighted the need to better understand NYC's changing flood hazard and emphasized the necessity of adaptation measures and resiliency planning to help protect against future flood events.

Five years after Sandy, coastal flooding remains a major concern for NYC, with nearly 50 million built square meters and 400,000 residents living within the current 100-year floodplain (PlaNYC 2013), and rates of local relative sea level rise (SLR) that exceed the global average (Miller et al. 2013; Engelhart et al. 2009; Kemp and Horton 2013). In a changing climate, the evolution of the coastal flood hazard for NYC will depend upon not only rising sea levels but also upon storm-surge events associated with hurricanes (where storm surge is defined as the atypical rise of water during a storm), which in turn will depend on changing storm characteristics (Garner et al. 2017; Reed et al. 2015; Lin et al. 2012, 2016; Little et al. 2015).

It is important to understand the ways in which storm surge events i) have already changed for NYC over the past millennium and ii) are likely to change in the future for a range of possible climates and physical assumptions (Reed et al. 2015; Garner et al. 2017). However, the brevity of the observational record of hurricanes in the Atlantic basin (extending from 1851 to the present), as well as potential biases in the record, presents a challenge to the accurate analysis of long-term trends in storm activity and severely limits the scope of potential investigations of coastal flood hazard associated with hurricanes (Kozar et al. 2013). Similarly, the instrumental record of sea level for NYC, recorded by the NOAA tide gauge network, goes back to only 1920.

We have worked to overcome the limitations of the relatively short observational record of Atlantic hurricanes by producing libraries of hundreds of years of synthetic storms under downscaled past and future climate simulations (Reed et al. 2015; Garner et al. 2017). For each of these storms, we generated storm surge heights at The Battery in NYC using the Advanced Circulation (ADCIRC) model, which predicts storm surge and flooding by solving the equations of motion for moving ocean waters on a rotating Earth (Luettich et al. 1992). We combined peak storm surge heights with proxy relative sea level records from New Jersey (850–2005 CE; Kemp and Horton 2013; Kemp et al. 2013) and with localized probabilistic SLR projections for NYC (2000-2300; Kopp et al. 2014, 2017) to estimate overall flood heights at The Battery from 850–2300 CE.

Generating synthetic storms

We generated synthetic hurricanes by downscaling a range of Coupled Model Intercomparison Project version 5 (CMIP5) models, focusing on the Last Millennium and representative concentration pathway (RCP) 8.5 simulations from three models: the Max-Planck-Institute (MPI) Earth System Model, the Coupled Climate System Model 4.0 (CCSM4), and the Institut Pierre Simon Laplace (IPSL) Earth System Model.

By essentially inserting a high-resolution hurricane model within the broader context of the relatively coarse-resolution global climate models, we generated a large number of hurricanes consistent with Last Millennium and future RCP 8.5 simulated climates (Emanuel et al. 2006, 2008; Kozar et al. 2013; Reed et al. 2015; Garner et al. 2017; Emanuel 2017). We filtered the hurricanes to focus on those that travel within 250 km of The Battery for the pre-industrial era (850–1800 CE; ~5000 storms from each model), modern era (1970–2005; ~5000 storms for each model), and the future (2010–2100 or 2300; ~12,000 storms per century for each model; Reed et al. 2015; Garner et al. 2017).

Driven by the trajectories, wind fields, and pressure fields of each of the synthetic hurricanes, we employed the ADCIRC model to project storm surges at The Battery (Lin et al. 2012; Reed et al. 2015; Garner et al. 2017; Lin et al. 2016). Storm surge was modeled on a 100 m resolution grid at The Battery (Lin et al. 2012; Reed et al. 2015; Garner et al. 2017). The ADCIRC model has previously been used to model and forecast storm surge events for coastal regions (e.g., Westerink et al. 2008; Colle et al. 2008; Lin et al. 2003; Dietrich et al. 2010).

Changing storm characteristics

Although modeled mean storm surge heights were not statistically different between the pre-industrial and modern eras, the largest and most extreme storm surge

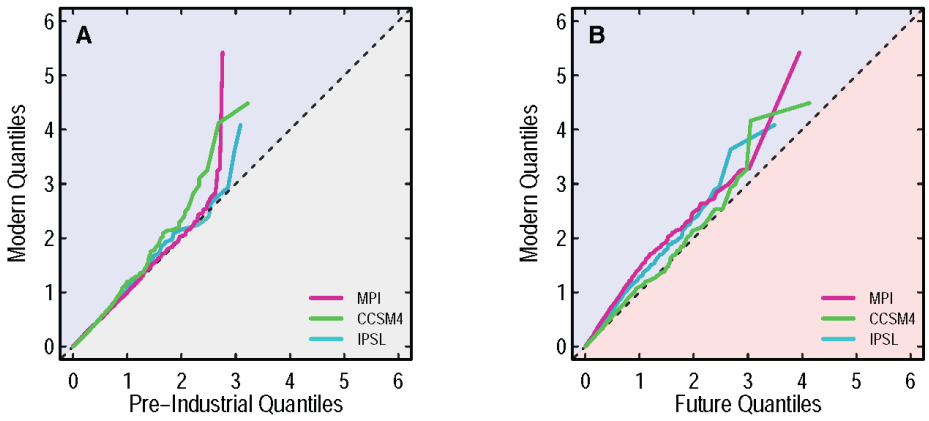

Figure 1. Quantile-Quantile plots of storm surge for a) the pre-industrial (gray) and modern (blue) eras, and b) the modern (blue) and future (red) eras for the MPI model (magenta), the CCSM4 model (green), and the IPSL model (cyan). The 1:1 line is shown by the black dashed line; points that deviate from this line indicate that the two distributions being compared differ from one another (e.g., points that fall into the blue portion of the figure indicate that modern storm surges for that portion of the distribution are greater than storm surges for that portion of the distribution from the other time period included on the plot).

events tended to be larger in the modern era than in the pre-industrial era (Figure 1; Reed et al. 2015). This result is not trivial, since such extreme events are likely to produce the most severe impacts for NYC (Aerts et al. 2013). A principal component analysis of the characteristics of storms impacting NYC for the pre-industrial and modern eras revealed that the largest storm surges at The Battery were generally caused by two different types of storms (Reed et al. 2015).

The first type of storm was characterized by large radius of maximum wind (RMW) (Reed et al. 2015). Although not necessarily intense, these hurricanes can be larger than average and, thus, can produce long-lived surges at The Battery, much as Sandy did in 2012 (Jones et al. 2003; Brandon et al. 2015). In this kind of event, the possibility of the storm surge overlapping with a high astronomical tide is heightened (Kemp and Horton 2013), meaning that overall flood heights may be exacerbated beyond those modeled in these studies (Reed et al. 2015).

The second type of storm was characterized by intensity. Although not necessarily large, these hurricanes have high maximum wind speeds and low minimum pressures (Reed et al. 2015). Storm surges from such events tend not to be as long-lived as surges from larger, less intense storms, but the winds and pressures associated with such hurricanes are capable of producing very large storm surge heights in NYC (Weisberg and Zheng 2015), similar to the surge that was observed during the Hurricane of 1938 (Landsea et al. 2014).

In future projections, hurricanes continued to become both more intense (increased maximum wind speeds and decreased minimum pressures) and potentially larger (increased RMW). Surprisingly, our analysis did not identify a corresponding increase in storm surge heights (Figure 1; Garner et al. 2017). This is because for future simulations hurricanes at the latitude of NYC tended to track farther eastward, staying farther out to sea than during the modern era (1980–2000; Figure 2). This shift in storm tracks compensated for the increase in hurricane size and intensity, resulting in little change or even slight decreases to storm surge heights at The Battery in the future (Garner et al. 2017). Such a shift in storm tracks is consistent with previous studies (Hall and Yonekura 2013; Baldini et al. 2016; Kossin et al. 2014; van Hengstum et al. 2016; Roberts et al. 2016). One possible explanation for this track shift may be changing sea level pressure fields, with projected future sea level pressures during August and September slightly higher over the US Atlantic coast and slightly lower over the North Atlantic than during the modern era (Garner et al. 2017).

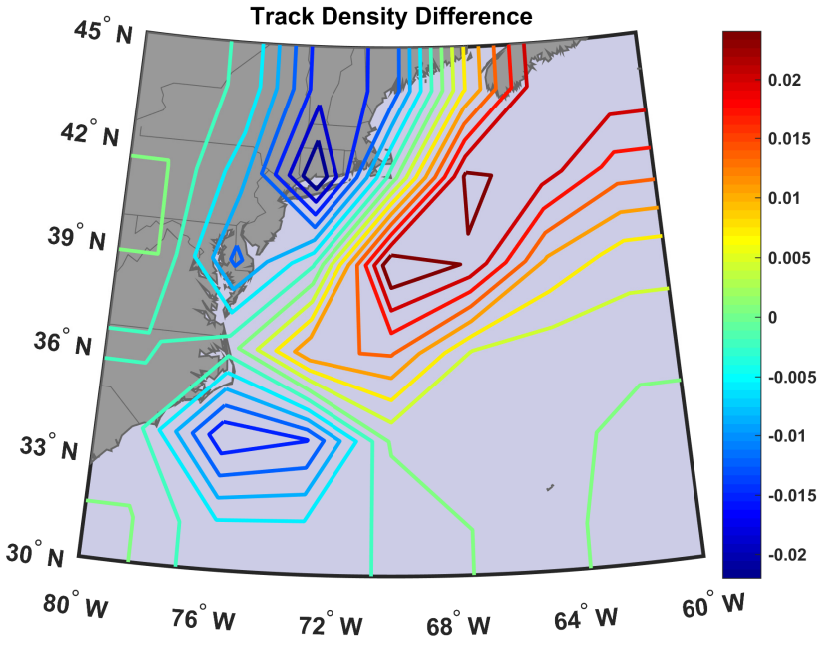

Figure 2. Multi-model mean difference between future and modern synthetic hurricane track densities from the MPI, CCSM4, and IPSL models. Track densities are determined by the sum total of tracks crossing through each grid box over 20-year periods from 2080–2100 and 1980–2000, divided by the area of that grid box and the number of years (21). Here the grid box latitude–longitude scales are determined by the output resolution of the model in question. Warmer colors (reds) indicate an increase in the number of future tracks relative to modern tracks, while cooler colors (blues) indicate a decrease in the number of future tracks relative to modern tracks. Figure from Garner et al. 2017.

The importance of rising sea levels

Flood heights are not determined by storm surge alone; they also include contributions from mean sea level, tidal variability, and wave action. In our analyses, we focused on the effects of storm surge and local relative sea level change.

We estimated overall flood height by linearly combining modeled peak storm surge heights with changes in mean sea level, as determined from proxy records (for the past) and localized probabilistic SLR projections (for the future) relative to a pre-industrial baseline. Non-linear effects of SLR on storm surge heights are expected to be small at The Battery (Lin et al. 2012; Orton et al. 2015), though it is possible that for very large amounts of SLR such a linear combination could result in an underestimate of the overall flood height (McKee Smith Ã et al. 2009; Zhang et al. 2013).

Relative SLR at The Battery for the pre-industrial era was estimated from proxy records taken from salt-marsh sediment cores from Cape May Courthouse and Leeds Point, New Jersey. These two reconstructions were combined to produce a single relative sea level record that accurately conveys multi-decadal to centennial-scale trends in relative sea level during the past two millennia (Kemp et al. 2013).

Future sea level at The Battery was based on localized, probabilistic projections from Kopp et al. (2014) for RCP 4.5 and 8.5, which included thermal expansion and ocean dynamics, glacier melt, ice sheet contributions, land water storage, non-climatic local sea level change, and gravitational effects on sea level. Under RCP 8.5, SLR by 2100 was 0.55-1.4 m and by 2300 was 1.5-5.7 m. Kopp's et al. (2014) central projections of Antarctic ice sheet contributions were based on those of IPCC AR5, with information about tail risk derived from a structured expert elicitation study. New research regarding ice-shelf hydrofracturing and ice-cliff collapse mechanisms suggest that these mechanisms have the potential to significantly increase the likelihood of extreme outcomes in the second half of this century and beyond (DeConto and Pollard, 2016). Thus, we also used two additional SLR projections for the RCP 4.5 and 8.5 scenarios with enhanced contributions from the Antarctic ice sheet (Kopp et al. 2017). The enhanced Antarctic ice sheet projections produced a SLR of 0.88-2.5 m and 10.7-15.7 m by 2100 and 2300, respectively, under RCP 8.5.

Despite the minimal change in storm surge, SLR (nearly 2 m in the region from the beginning of the pre-industrial era to the end of the modern era; see Figure 1 in Reed et al., 2015) caused a large increase in the flood hazard for NYC from the pre-industrial to the modern era (Figure 3). For example, a flood height with a return period of 500 years was 2.25 m during the pre-industrial era; this increased to 3.3-3.7 m during the modern era. In addition, the return period of the 2.25 m flood decreased from 500

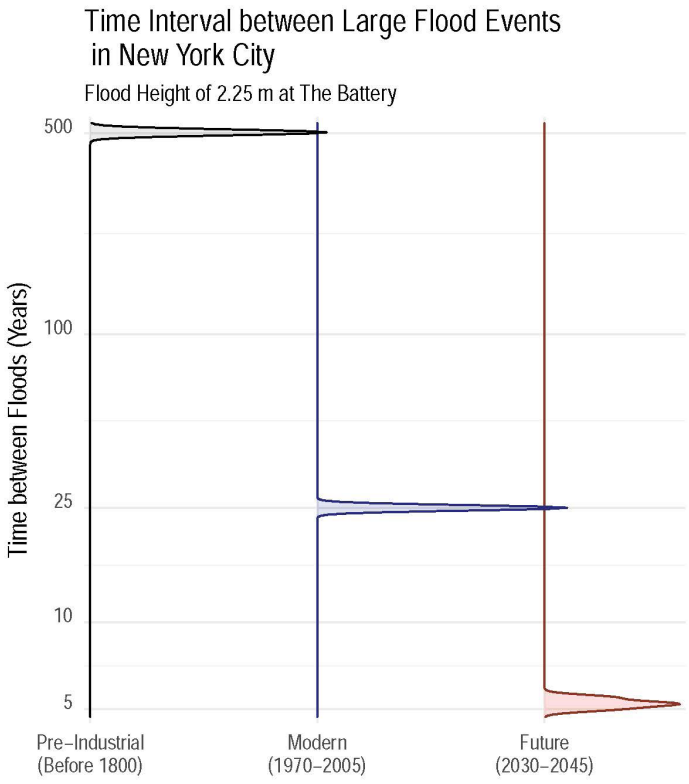

Figure 3. Return periods of the 2.25 m flood height at The Battery for the pre-industrial era (gray), modern era (blue), and future era (red).

years to ~25 years during the transition from the pre-industrial to modern era (Reed et al., 2015).

The late 21st and 23rd centuries show dramatic increases in flood hazard especially under the RCP 8.5 scenario with rapid collapse of the Antarctic ice sheet. The 500-year flood height increased to 4.0-5.1 m by the end of the 21st century and 5.0-15.4 m by the end of the 23rd century. The 2.25 m flood decreased to approximately five years by 2030-2045 in our simulations (Figure 3; Garner et al. 2017).

Evolving flood risk

From the pre-industrial era to the modern era, the increased coastal flood hazard in NYC was driven by local relative SLR and increases in the extremes of the types of storms — large and intense — that cause the most destructive storm surge flooding for the region (Reed et al. 2015). In the future, though storm size and intensity are projected to increase, overall storm surge heights will remain unchanged in NYC because of an eastward shift in storm tracks (Garner et al. 2017). We note that the possibility remains for a very rare event in which a damaging storm breaks this pattern by traveling directly over NYC. Ultimately, flood hazard will continue to increase in the future, with SLR playing a significant role in determining the magnitude.

Because sea level responds relative to a changing climate on long timescales, NYC is already committed to future SLR. Therefore, the findings from this study suggest that it is imperative to invest in adaptation strategies to help make NYC's infrastructure more resilient to future flooding, in order to protect the property and residents living within the current 100-year flood plain (PlaNYC 2013). The results presented here also provide hope for NYC. Given the dominant role of SLR in increased future flood risk, our results suggest that by taking appropriate steps both now and in the coming decades to mitigate climate change we may be able to avoid the worst-case scenarios.

References

Aerts, J. C. J. H., N. Lin, W. J. Wouter Botzen, K. Emanuel, and H. De Moel, 2013: Low-probability flood risk modeling for New York City. *Risk Anal.*, **33**, 772–778, doi:10.1111/risa.12008.

Baldini, L. M., and Coauthors, 2016: Persistent northward North Atlantic tropical cyclone track migration over the past five centuries. *Sci. Rep.*, **6**, 37522, doi:10.1038/srep37522.

Blake, E. S., T. B. Kimberlain, R. J. Berg, J. P. Cangialosi, and J. L. Beven, 2013: *Tropical Cyclone Report: Hurricane Sandy (AL182012) 22 - 29 October 2012,* http://www.nhc.noaa.gov/data/tcr/AL182012_Sandy.pdf.

Brandon, C. M., J. D. Woodruff, J. P. Donnelly, and R. M. Sullivan, 2015: How unique was Hurricane Sandy? Sedimentary reconstructions of extreme flooding from New York Harbor. *Sci. Rep.*, **4**, 7366, doi:10.1038/srep07366.

Colle, B. A., F. Buonaiuto, M. J. Bowman, R. E. Wilson, R. Flood, R. Hunter, A. Mintz, and D. Hill, 2008: Advances in high-resolution storm surge modeling for the New York City metropolitan region should help forecasters and emergency managers during an impending storm. Storm Surge Modeling of Past Cyclones. *Bull. Amer. Meteorol. Soc.*, **89**, 829–841, doi:10.1175/2007BAMS2401.1.

DeConto, R. M., and D. Pollard, 2016: Contribution of Antarctica to past and future sea-level rise. *Nature*, **531**, 591–597, doi:10.1038/nature17145.

Dietrich, J. C., and Coauthors, 2010: Modeling hurricane waves and storm surge using integrally-coupled, scalable computations. *Coast. Eng.*, **58**, 45–65, doi:10.1016/j.coastaleng.2010.08.001.

Emanuel, K., 2017: Assessing the present and future probability of Hurricane Harvey's rainfall. *Proc. Natl. Acad. Sci.* doi:10.1073/pnas.1716222114.

Emanuel, K., S. Ravela, E. Vivant, C. Risi, K. Emanuel, S. Ravela, E. Vivant, and C. Risi, 2006: A statistical deterministic approach to hurricane risk assessment. *Bull. Amer. Meteorol. Soc.*, **87**, 299–314, doi:10.1175/BAMS-87-3-299.

Emanuel, K., R. Sundararajan, and J. Williams, 2008: Hurricanes and global warming: Results from downscaling IPCC AR4 simulations. *Bull. Amer. Meteorol. Soc.*, **89**, 347–367, doi:10.1175/BAMS-89-3-347.

Engelhart, S. E., B. P. Horton, B. C. Douglas, W. R. Peltier, and T. E. Tornqvist, 2009: Spatial variability of late Holocene and 20th century sea-level rise along the Atlantic coast of the United States. *Geology*, **37**, 1115–1118, doi:10.1130/G30360A.1.

Garner, A. J., and Coauthors, 2017: Impact of climate change on New York City's coastal flood hazard: Increasing flood heights from the preindustrial to 2300 CE. *Proc. Natl. Acad. Sci.*, doi:10.1073/pnas.1703568114.

Hall, T., and E. Yonekura, 2013: North American tropical cyclone landfall and SST: A statistical model Study. *J. Climate*, **26**, 8422–8439, doi:10.1175/JCLI-D-12-00756.1.

van Hengstum, P. J., J. P. Donnelly, P. L. Fall, M. R. Toomey, N. A. Albury, and B. Kakuk, 2016: The intertropical convergence zone modulates intense hurricane strikes on the western North Atlantic margin. *Sci. Rep.*, **6**, doi:10.1038/srep21728.

Jones, S. C., and Coauthors, 2003: The extratropical transition of tropical cyclones: Forecast challenges, current understanding, and future directions. *Wea. Forecast.*, **18**, 1052–1092, doi:10.1175/1520-0434(2003)018<1052:TETOTC>2.0.CO;2.
Kemp, A. C., and B. P. Horton, 2013: Contribution of relative sea-level rise to historical hurricane flooding in New York City. *J. Quat. Sci.*, **28**, 537–541, doi:10.1002/jqs.2653.
Kemp, A. C., and Coauthors, 2013: Sea-level change during the last 2500 years in New Jersey, USA. *Quat. Sci. Rev.*, **81**, 90–104, doi:10.1016/j.quascirev.2013.09.024.
Kopp, R. E., R. M. Horton, C. M. Little, J. X. Mitrovica, M. Oppenheimer, D. J. Rasmussen, B. H. Strauss, and C. Tebaldi, 2014: Probabilistic 21st and 22nd century sea-level projections at a global network of tide-gauge sites. *Earth's Futur*, **2**, 383–406, doi:10.1002/2014EF000239.
Kopp, R. E., and Coauthors, 2017: Evolving understanding of Antarctic ice-sheet physics and ambiguity in probabilistic sea-level projections. *arXiv,* http://arxiv.org/abs/1704.05597.
Kossin, J. P., K. A. Emanuel, and G. A. Vecchi, 2014: The poleward migration of the location of tropical cyclone maximum intensity. *Nature*, **509**, 349–352, doi:10.1038/nature13278.
Kozar, M. E., M. E. Mann, K. A. Emanuel, and J. L. Evans, 2013: Long-term variations of North Atlantic tropical cyclone activity downscaled from a coupled model simulation of the last millennium. *J. Geophys. Res. Atmos.*, **118**, 13,383-13,392, doi:10.1002/2013JD020380.
Landsea, C. W., A. Hagen, W. Bredemeyer, C. Carrasco, D. A. Glenn, A. Santiago, D. Strahan-Sakoskie, and M. Dickinson, 2014: A reanalysis of the 1931–43 Atlantic hurricane database*. *J. Climate*, **27**, 6093–6118, http://www.aoml.noaa.gov/hrd/Landsea/landsea-et-al-jclimate-2014.pdf.
Lin, N., J. A. Smith, G. Villarini, T. P. Marchok, and M. L. Baeck, 2003: Modeling extreme rainfall, winds, and surge from Hurricane Isabel. *Wea. Forecast.*, **25**, 1342–1361, doi:10.1175/2010WAF2222349.1.
Lin, N., K. Emanuel, M. Oppenheimer, and E. Vanmarcke, 2012: Physically based assessment of hurricane surge threat under climate change. *Nature Climate Change*, **2**, 462–467, doi:10.1038/nclimate1389.
Lin, N., R. E. Kopp, B. P. Horton, and J. P. Donnelly, 2016: Hurricane Sandy's flood frequency increasing from year 1800 to 2100. *Proc. Natl. Acad. Sci.*, **113**, 12071–12075, doi:10.1073/pnas.1604386113.
Little, C. M., R. M. Horton, R. E. Kopp, M. Oppenheimer, G. A. Vecchi, and G. Villarini, 2015: Joint projections of US East Coast sea level and storm surge. *Nature Climate Change*, **5**, 1114–1120, doi:10.1038/nclimate2801.
Luettich, R. A. J., J. J. Westerink, and N. W. Scheffner, 1992: ADCIRC: An advanced three-dimensional circulation model for shelves, coasts, and estuaries. *Report 1. Theory and Methodology of ADCIRC-2DDI and ADCIRC-3DL*, Department of the Amry, Technical Report DRP 92-6, http://www.dtic.mil/docs/citations/ADA261608.
McKee Smith Ã, J., M. A. Cialone, T. V Wamsley, and T. O. McAlpin, 2009: Potential impact of sea level rise on coastal surges in southeast Louisiana. *Ocean Eng.*, **37**, 37–47, doi:10.1016/j.oceaneng.2009.07.008.
Miller, K. G., R. E. Kopp, B. P. Horton, J. V. Browning, and A. C. Kemp, 2013: A geological perspective on sea-level rise and its impacts along the U.S. mid-Atlantic coast. *Earth's Future*, **1**, 3–18, doi:10.1002/2013EF000135.
Orton, P., and Coauthors, 2015: New York City Panel on Climate Change 2015 Report Chapter 4: Dynamic Coastal Flood Modeling. *Ann. N.Y. Acad. Sci.*, **1336**, 56–66, doi:10.1111/nyas.12589.
PlaNYC 2013: *A stronger, more resilient New York*. New York City, 455 pp. http://www.nyc.gov/html/sirr/html/report/report.shtml.
Reed, A. J., M. E. Mann, K. A. Emanuel, N. Lin, B. P. Horton, A. C. Kemp, and J. P. Donnelly, 2015: Increased threat of tropical cyclones and coastal flooding to New York City during the anthropogenic era. *Proc. Natl. Acad. Sci.*, **112**, 12610–12615, doi:10.1073/pnas.1513127112.
Roberts, K. J., B. A. Colle, and N. Korfe, 2016: Impact of simulated twenty-first-century changes in extratropical cyclones on coastal flooding at the Battery, New York City. *J. Appl. Meteorol. Climatol.*, **56**, 415–432, doi:10.1175/JAMC-D-16-0088.1.
Weisberg, R. H., and L. Zheng, 2006: Hurricane Storm Surge Simulations for Tampa Bay. *Estuar. Coasts*, **29**, 899–913, doi:10.2307/4124819.
Westerink, J. J., and Coauthors, 2008: A basin-to channel-scale unstructured grid hurricane storm surge model applied to southern Louisiana. *Mon. Wea. Rev.*, **136**, 833–864, doi:10.1175/2007MWR1946.1.
Zhang, K., Y. Li, H. Liu, H. Xu, and J. Shen, 2013: Comparison of three methods for estimating the sea level rise effect on storm surge flooding. *Climate Change*, **118**, 487–500, doi:10.1007/s10584-012-0645-8.

Learn more about US CLIVAR's 20th Anniversary and contribute a testimonial!

Global distribution of projected dynamic ocean sea level changes using multiple climate models and economic assessment of sea level rise

Hiromune Yokoki, Makoto Tamura, Mizuki Yotsukuri, Naoko Kumano, and Yuji Kuwahara

Ibaraki University, Japan

In recent years, many climate models have been developed, providing reliable parameters related to future climate changes, most of which have been adopted in the United Nation's Intergovernmental Panel on Climate Change assessment reports (IPCC 2014). However, the relevant outputs for sea level changes provided by these models do not perfectly coincide with each other. This might create an obstacle to practical studies on the impacts of and adaptations to climate change. Even though there are uncertainties associated with the projected sea level rise (SLR), it is quite important to assess various impacts, such as inundation, using these models in order to consider appropriate adaptation options and to estimate their costs.

In this article, we summarize the results of a study intended to assess potential areas of future inundation using the global distribution of dynamic sea level changes (including global averaged ocean thermal expansion but not changes in mass of the ocean from glaciers or ice sheets) projected by selected climate models, and estimate the population affected and economic damages to coastal zones around the world.

Methodology

Of the various climate model products relevant to sea level changes provided for CMIP5, the outputs of four models (CanESM2, MIROC-ESM, MPI-ESM-MR, and NorESM1-M) were selected to compare projected sea level changes. Using these outputs, the variances in global mean thermal expansion and the differences in distribution patterns of sea level changes based on the same Representative Concentration Pathways (RCP) scenarios (RCP2.6, RCP4.5, and RCP8.5) were investigated. Temporal changes in sea level were also investigated for each of the RCP scenarios.

Inundation damage in coastal zones is considered to be a significant consequence of SLR. Potentially inundated areas and their temporal changes were estimated using topographic data (ETOPO1) and sea surface height data, which were adjusted vertically to the geoid. ETOPO1, which provides elevation data on land surface and sea bottom in a 1 arc-minute global relief model of the Earth's surface that integrates land topography and ocean bathymetry (Amante and Eakins 2009), was smoothed using a weighted 2.5 arc-minute gridded resolution. Astronomical high tides were included in the calculations of the sea surface height, but storm surges were not, since the study focused on impacts of daily inundation rather than occasional extreme events.

Steric sea surface height data and other outputs of CMIP5 were obtained from the database of the National Institute for Environmental Studies, Japan (NIES 2016). Global tidal data were obtained from TPXO7.2 (Egbert and Erofeeva

2002). High tide during a spring tide was combined with the four major component tides (M2, K1, S2, and O1).

Comparisons of sea surface height and land elevation were used to identify potentially inundated areas. Because there aren't accurate and consistent elevation data or maps of already installed dikes in coastal areas of the world, we globally estimated the potentially inundated area without considering coastal structures, such as dikes. By applying the various shared socioeconomic pathways (SSP) scenarios — a set of alternative futures of societal development — (O'Neill et al. 2017) to the predicted inundated area, the affected population and associated economic damage were estimated. For the SSP scenarios (SSP1-3), a 0.5 arc-degree gridded resolution was used for population and GDP projections, which were rescaled by Murakami and Yamagata (2016). The downscaled SSPs include the effects of urban shrinkage/dispersion related to socioeconomic scenarios but do not consider movement due to evacuation from urgent inundation.

A macro estimation method was used to evaluate the economic impact of inundation. Following the approach of Yotsukuri et al. (2017), economic damage estimates were based on the econometric relationship between past hydrological disasters, the affected population, and per capita GDP using the Centre for Research on the Epidemiology of Disasters (CRED) Emergency Events Database (EM-DAT; CRED 2016) and the World Bank's national statistics. Unless otherwise specified, all monetary values have been converted to 2005 US dollars and were not discounted, as in Hinkel et al. (2014).

Results

Figure 1 compares the global average SLR projection (from thermal expansion only) relative to 2006 for the four climate models. MIROC-ESM (Watanabe et al. 2011) gave the largest SLR for all the RCPs, ranging from about 30 to 50 cm in 2100, and NorESM1-M showed the second largest steric SLR. MPI-ESM-MR and CanESM2 exhibited nearly the same average SLR. The remaining analyses were examined using the maximum impacts, i.e., MIROC-ESM.

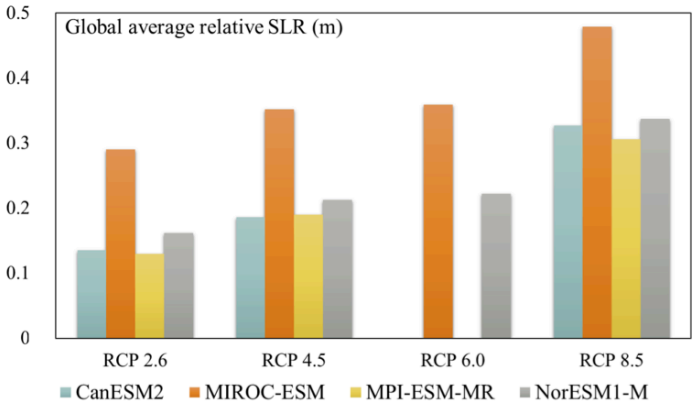

Figure 1. Comparison of global average SLR from thermal expansion only for four climate models under RCP scenarios of 2.6, 4.5, 6.0, and 8.5.

Figure 2 presents potentially inundated areas with and without high tides. The regional distribution of astronomical high tides, which are about 41 cm on average, was included in the calculations. Without astronomical high tides, the potentially inundated areas varied from 119,000 km^2 (RCP2.6) to 163,000 km^2 (RCP8.5) in 2100. With high tides, the potentially inundated areas varied from 370,000 km^2 (RCP2.6) to 420,000 km^2 (RCP8.5). Countries with the largest potentially inundated areas included China, Canada, Vietnam, the United States, Brazil, Australia, Indonesia, and India

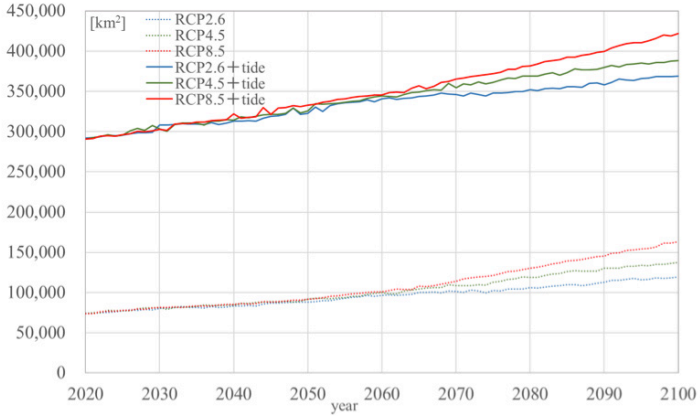

Figure 2. Potentially inundated areas (km^2) of the global coastline with (solid lines) and without (dotted lines) high tides under the RCP scenarios of 2.6, 4.5, and 8.5.

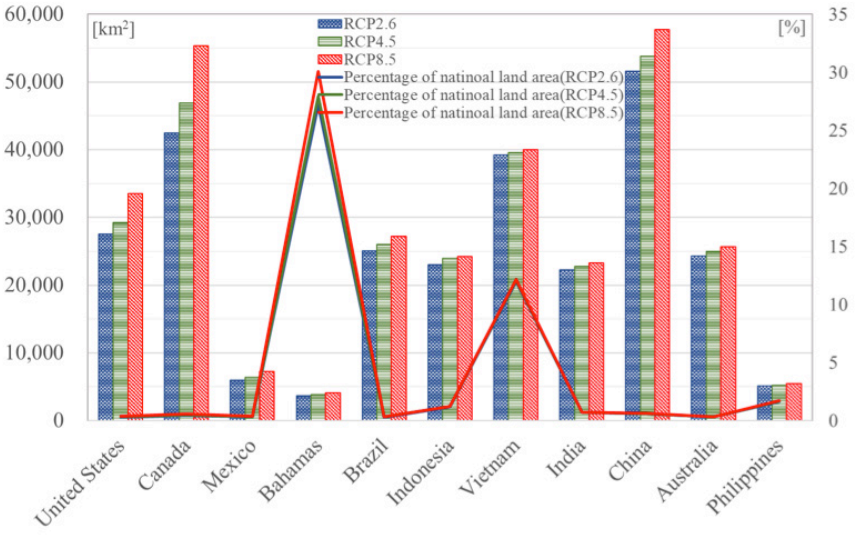

Figure 3. Potentially inundated area (km², dashed bars) and its percentage of national land area (lines) for various countries in 2100.

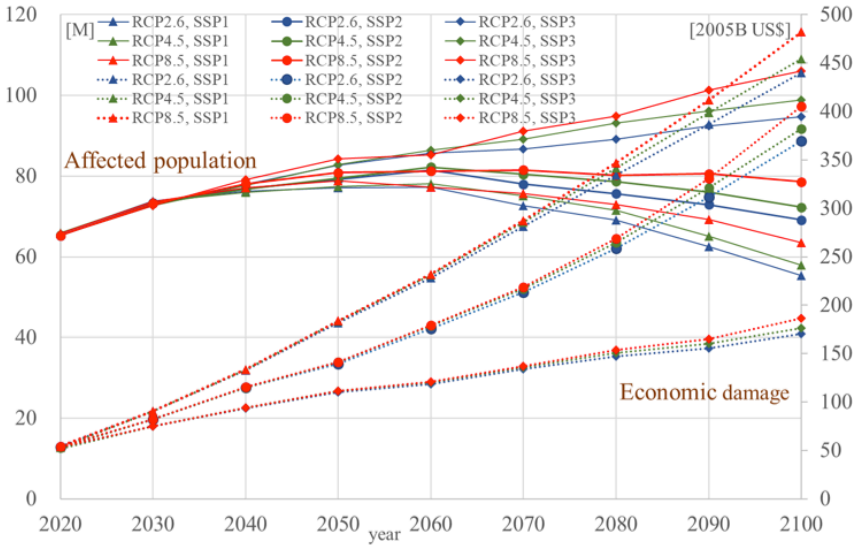

Figure 4. Affected population (solid; left-side axis; millions) and economic damage (dotted; right-side axis; billions USD) due to SLR and high tides (SSP1; triangles, SSP2; circles, SSP3; rhombuses).

(Figure 3). In contrast, countries with the largest percentage of inundated lands included the Bahamas, Vietnam, and the Philippines. It is necessary to consider both absolute and relative impacts according to the size of countries.

Figure 4 presents the population affected with high tides, which varies from 55.3 million (RCP2.6, SSP1) to 106 million (RCP8.5, SSP3). Probabilistic combinations of RCP and SSP were not considered here. Although combinations of RCP8.5 and SSP1 or RCP2.6 and SSP3 may be rare, the study presents the range between the minimum and maximum impacts. Probability analysis will be conducted in subsequent studies. Figure 4 also shows the economic damage estimates based on the three damage functions, which varies from 169 billion (RCP2.6, SSP3) to 482 billion US$ (RCP8.5, SSP1) in 2100. RCP8.5 showed the largest affected population and economic damage under the same SSP. SSP3 ("regional rivalry") resulted in the largest affected population in 2100, followed by SSP2 ("middle of the road") and SSP1 ("sustainability") under the same RCP. The affected population in SSP1 decreased after 2060 because its world population peaks at around 2060. On the other hand, SSP1 resulted in the largest economic damage in 2100, followed by SSP2 and SSP3. Socioeconomic impacts, such as the size of the affected population and the extent of economic damage, were more dependent on SSP than RCP.

Conclusion

The global distribution of projected inundation impacts and temporal changes in steric SLR-induced inundation, including

astronomical high tides, were assessed. Combining the results of inundated areas based on RCP scenarios with SSP scenarios using the Earth system model MIROC-ESM, the populations affected and the economic damages caused by inundation due to future climate change scenarios were also estimated. With high tides, the potentially inundated areas varied from 370,000 km^2 (RCP2.6) to 420,000 km^2 (RCP8.5) and the affected population varied from 55.3 million (RCP2.6, SSP1) to 106 million (RCP8.5, SSP3) in 2100. Socioeconomic impacts, such as the size of the affected population and economic damage, were more dependent on SSP than RCP. Though the projection of SLR includes only ocean dynamic sea level in this study (not including changes in ocean mass), such global analysis will enable to the comparison of differences in various damages in countries and provide a basis for discussing appropriate country-specific as well as global adaptations in international debates.

Acknowledgements

Earlier versions of this study were presented at the WCRP/IOC Sea Level Conference (Yokoki et al. 2017) and in Yotsukuri et al. (2017). This study was supported by the Environment Research and Technology Development Fund (S-14 and 2-1712) of the Ministry of the Environment and a Grant-in-Aid for Scientific Research (B: 26281055) from MEXT, Japan.

References

Amante, C. and B. W. Eakins, 2009: ETOPO1: 1 Arc-minute global relief model: procedures, data sources and analysis. NOAA Technical Memorandum, NESDIS NGDC-24, 19pp. https://www.ngdc.noaa.gov/mgg/global/relief/ETOPO1/docs/ETOPO1.pdf.

CRED, 2016: EM-DAT: The international disaster database. http://www.emdat.be/.

Egbert, G. D., and S. Y. Erofeeva, 2002: Efficient inverse modeling of Barotropic ocean tides. *J. Atmos. Ocean. Tech*., **19**, 183-204, doi:10.1175/1520-0426(2002)019<0183:EIMOBO>2.0.CO;2.

Hinkel, J., D. Lincke, A. T. Vafeidis, M. Perrette, R. J. Nicholls, R. S. J. Tol, B. Marzeion, X. Fettweis, C. Ionescu, and A. Levermann, 2014: Coastal flood damage and adaptation costs under 21st century sea-level rise. *Proc. Nat. Acad. Sci.*, **111**, 3292-3297, doi: 10.1073/pnas.1222469111.

IPCC, 2014: Climate Change 2014: Impacts, Adaptation, and Vulnerability. Part A: Global and Sectoral Aspects. Contribution of Working Group II to the Fifth Assessment Report of the Intergovernmental Panel on Climate Change, Field, C.B., V.R. Barros, D.J. Dokken, K.J. Mach, M.D. Mastrandrea, T.E. Bilir, M. Chatterjee, K.L. Ebi, Y.O. Estrada, R.C. Genova, B. Girma, E.S. Kissel, A.N. Levy, S. MacCracken, P.R. Mastrandrea, and L.L.White, Eds. Cambridge University Press, Cambridge, United Kingdom and New York, NY, USA, 1132 pp., http://www.ipcc.ch/report/ar5/wg2/.

Murakami, D. and Y. Yamagata, 2016: Estimation of gridded population and GDP scenarios with spatially explicit statistical downscaling, arXiv:1610.09041.

NIES, 2016: Global meteorological data server, http://h08.nies.go.jp/ddc/.

O'Neill, B. C., E. Kriegler, K. L. Ebi, E. Kemp-Benedict, K. Riahi, D. S. Rothman, B. J. van Ruijven, D. P. van Vuuren, and J. Birkmann, 2017: The roads ahead: Narratives for shared socioeconomic pathways describing world futures in the 21st century. *Glob. Environ. Chan.*, **42**, 169-180, doi: 10.1016/j.gloenvcha.2015.01.004.

Watanabe S., and Coauthors, 2011: MIROC-ESM 2010: Model description and basic results of CMIP5-20c3m experiments. *Geosci. Mod. Dev*., **4**, 845-872, doi:10.5194/gmd-4-845-2011.

Yokoki, H., M. Tamura, and Y. Kuwahara, 2017: Global distribution of projected sea level changes using multiple climate models and economic assessment of sea level rise. International WCRP/IOC Conference 2017, Regional Sea Level Changes and Coastal Impacts. Columbia University, USA, July 12, 2017.

Yotsukuri, M., M. Tamura, N. Kumano, E. Masunaga, and H. Yokoki, 2017: Global impact assessment of sea level rise based on RCP/SSP scenarios. *J. Japan Soc. Civ. Eng.* (Environment) **73**, 369-376, https://ci.nii.ac.jp/naid/40021334522/, (in Japanese).

Read the 2017 Sea Level Conference Statement

Image credit: Kristan Uhlenbrock

International CLIVAR Project Office
First Institute of Oceanography, SOA,
6 Xianxialing Road, Laoshan District, Qingdao
266061,China
icpo@clivar.org
http://www.clivar.org
twitter.com/wcrp_clivar

US CLIVAR Project Office
1201 New York Ave. NW, Suite 400
Washington, DC 20005
(202) 787-1682
uscpo@usclivar.org
www.usclivar.org
twitter.com/usclivar

CLIVAR is the World Climate Research Programme's (WCRP) core project on the ocean-atmosphere system.

WCRP is sponsored by the World Meteorological Organization, the International Council for Science, and the Intergovernmental Oceanographic Commission of UNESCO. The ICPO is supported by China State Oceanographic Administration /First Institute of Oceanography (FIO) and the Indian Ministry of Earth Sciences/ Indian Institute of Tropical Meteorology (IITM).

US CLIVAR acknowledges support from these US agencies:

This material was developed with federal support of NASA and NSF (AGS-1502208), NOAA (NA11OAR4310213), and DOE (DE-SC0016332). Any opinions, findings, conclusions, or recommendations expressed in this material are those of the authors and do not necessarily reflect the views of the sponsoring agencies.